AFGL-TR-88-0025 TGAL-88-01

INVESTIGATION OF EXPLOSION GENERATED SV Lg WAVES IN 2-D HETEROGENEOUS CRUSTAL MODELS BY FINITE-DIFFERENCE METHOD

Rong-Song Jih
Keith L. McLaughlin

Teledyne Geotech Alexandria Laboratories
314 Montgomery Street
Alexandria, VA 22314-1581

FEBRUARY 1988

SCIENTIFIC REPORT #2

AIR FORCE GEOPHYSICS LABORATORY
AIR FORCE SYSTEMS COMMAND
UNITED STATES AIR FORCE
HANSCOM AIR FORCE BASE, MASSACHUSETTS 01731

Sponsored by: Defense Advanced Research Projects Agency
Nuclear Monitoring Research Office

DARPA Order No. 5307

Monitored by: Air Force Geophysics Laboratory

Contract No. F19628-86-C-0054

"This technical report has been reviewed and is approved for publication."

JAMES F. LEWKOWICZ
Contract Manager

HENRY A. OSSING
Chief, Solid Earth Geophysics Branch

FOR THE COMMANDER

DONALD H. ECKHARDT
Director
Earth Sciences Division

This report has been reviewed by the ESD Public Affairs Office (PA) and is releasable to the National Technical Information Service (NTIS).

Qualified requestors may obtain additional copies from the Defense Technical Information Center. All others should apply to the National Technical Information Service.

If your address has changed, or if you wish to be removed from the mailing list, or if the addressee is no longer employed by your organization, please notify AFGL/DAA, Hanscom AFB, MA 01731. This will assist us in maintaining a current mailing list.

Do not return copies of this report unless contractual obligations or notices on a specific document requires that it be returned.

Unclassified
SECURITY CLASSIFICATION OF THIS PAGE

REPORT DOCUMENTATION PAGE

Form Approved
OMB No 0704 0188
Exp Date Jun 30 1986

1a REPORT SECURITY CLASSIFICATION Unclassified	1b RESTRICTIVE MARKINGS
2a SECURITY CLASSIFICATION AUTHORITY	3 DISTRIBUTION / AVAILABILITY OF REPORT Approved for public release; Distribution unlimited.
2b DECLASSIFICATION / DOWNGRADING SCHEDULE	
4 PERFORMING ORGANIZATION REPORT NUMBER(S) TGAL-88-01	5 MONITORING ORGANIZATION REPORT NUMBER(S) AFGL-TR-88-0025
6a NAME OF PERFORMING ORGANIZATION Teledyne Geotech 6b OFFICE SYMBOL (If applicable) TGAL	7a NAME OF MONITORING ORGANIZATION Air Force Geophysics Laboratory
6c ADDRESS (City, State, and ZIP Code) 314 Montgomery Street Alexandria, VA 22314	7b ADDRESS (City, State, and ZIP Code) Hanscom AFB, MA 01731-5000
8a NAME OF FUNDING / SPONSORING ORGANIZATION Air Force Geophysics Lab. 8b OFFICE SYMBOL (If applicable) DSO/GSD	9 PROCUREMENT INSTRUMENT IDENTIFICATION NUMBER F19628-86-C-0054
8c ADDRESS (City, State, and ZIP Code) Hanscom AFB, MA 01731-5000	10 SOURCE OF FUNDING NUMBERS PROGRAM ELEMENT NO: 62714E; PROJECT NO: 6A10; TASK NO: DA; WORK UNIT ACCESSION NO: BC

11 TITLE (Include Security Classification)
INVESTIGATION OF EXPLOSION GENERATED SV Lg WAVES IN 2-D HETEROGENEOUS CRUSTAL MODELS BY FINITE-DIFFERENCE METHOD

12 PERSONAL AUTHOR(S)
Rong-Song Jih and K. L. McLaughlin

13a TYPE OF REPORT	13b TIME COVERED	14 DATE OF REPORT (Year, Month, Day)	15 PAGE COUNT
Scientific #2	FROM May 1987 TO Feb 1988	February 1988	80

16 SUPPLEMENTARY NOTATION

17 COSATI CODES			18 SUBJECT TERMS (Continue on reverse if necessary and identify by block number)
FIELD	GROUP	SUB-GROUP	Finite-Difference, ~~P-wave~~ ~~Lg-wave~~ SOILS, NOISE
			Topography, Seismology, Heterogeneity.

19 ABSTRACT (Continue on reverse if necessary and identify by block number)

A linear finite-difference (FD) method was used to compare the excitation of far-field P- and SV-waves generated by shallow dilatational sources in a suite of heterogeneous 2-D crustal models. The crustal models tested included simple layered structures, media with random velocity perturbations having Gaussian or self-similar autocorrelation functions, media with rough or gentle topography generated by Markov chains, and laminated media with sinusoidal folds. The numerical experiments were conducted by directing a broadband planar P- or SV-wave with appropriate incidence angle upon the testing models. The dilatational strain history at a shallow linear array of grid points was then recorded so that the far-field P- or SV(Lg)-waves from shallow dilatational sources could be inferred by use of the principle of reciprocity. The raw FD synthetics were deconvolved so as to represent the response due to explosion sources with a fixed yield. The mean peak amplitude of the synthetics for each model are compared to that for a reference model consisting of a simple layered medium. The average energy content in an appropriate signal window was measured as a complement to the amplitude meas-

20 DISTRIBUTION / AVAILABILITY OF ABSTRACT	21 ABSTRACT SECURITY CLASSIFICATION	
[ ] UNCLASSIFIED/UNLIMITED [ ] SAME AS RPT [ ] DTIC USERS	Unclassified	
22a NAME OF RESPONSIBLE INDIVIDUAL James F. Lewkowicz	22b TELEPHONE (Include Area Code) (617) 377-3028	22c OFFICE SYMBOL AFGL/LWH

DD FORM 1473, 84 MAR — 83 APR edition may be used until exhausted. All other editions are obsolete.

SECURITY CLASSIFICATION OF THIS PAGE
Unclassified

(19. continued)

urement. Both approaches show essentially the same pattern of P/SV excitation, namely that models with topography consistently produce the strongest P-SV conversion among all types of crustal models. The introduction of interfaces (*e.g.*, dipping layers) alone does not by itself increase SV excitation with the required slowness range. Thus $m_b(P)$ - $m_b(Lg)$ appears to be smaller for models with topographic relief (*e.g.*, the Novaya Zemlya Island) than for models with dipping layers or folded sedimentary rocks (*e.g.*, Shagan River, eastern EKTS).

These synthetic results are consistent with observations for Novaya Zemlya (Nuttli, 1988) and Shagan River (Nuttli,1986), based on WWSSN film chip readings of Lg. The Novaya Zemlya, which has rough topography, has a higher Lg relative to P ($m_b(P)$ - $m_b(Lg)$ = 0.04) than does the somewhat flatter Shagan River test site ($m_b(P)$ - $m_b(Lg)$ = 0.27). However, Nuttli (1987) also obtained relatively low $m_b(Lg)$ for the Degelen Test Site, which is only 70 km away from Shagan River. If this Degelen-Shagan River bias is real, it is not explained by the FD results obtained to date. However, some recently archived high-quality digital seismograms recorded at the Chinese Digital Seismic Network indicate more Lg excitation (with respect to P) at Degelen than at Shagan River, which is consistent with our numerical results.

INVESTIGATION OF EXPLOSION GENERATED SV Lg WAVES IN 2-D HETEROGENEOUS CRUSTAL MODELS BY FINITE-DIFFERENCE METHOD

SUMMARY

A linear finite-difference (FD) method was used to compare the excitation of far-field P- and SV-waves generated by shallow dilatational sources in a suite of heterogeneous 2-D crustal models. The crustal models tested included simple layered structures, media with random velocity perturbations having Gaussian or self-similar autocorrelation functions, media with rough or gentle topography generated by Markov chains, and laminated media with sinusoidal folds. The numerical experiments were conducted by directing a broadband planar P- or SV-wave with appropriate incidence angle upon the testing models. The dilatational strain history at a shallow linear array of grid points was then recorded so that the far-field P- or SV(Lg)-waves from shallow dilatational sources could be inferred by use of the principle of reciprocity. The raw FD synthetics were deconvolved so as to represent the response due to explosion sources with a fixed yield. The mean peak amplitude of the synthetics for each model are compared to that for a reference model consisting of a simple layered medium. The average energy content in an appropriate signal window was measured as a complement to the amplitude measurement. Both approaches show essentially the same pattern of P/SV excitation, namely that models with topography consistently produce the strongest P-SV conversion among all types of crustal models. The introduction of interfaces (*e.g.*, dipping layers) alone does not by itself increase SV excitation with the required slowness range. Thus $m_b(P)$ - $m_b(Lg)$ appears to be smaller for models with topographic relief (*e.g.*, the Novaya Zemlya Island) than for models with dipping layers or folded sedimentary rocks (*e.g.*, Shagan River, eastern EKTS).

These synthetic results are consistent with observations for Novaya Zemlya (Nuttli, 1988) and Shagan River (Nuttli,1986), based on WWSSN film chip readings of Lg. The Novaya Zemlya, which has rough topography, has a higher Lg relative to P ($m_b(P)$ - $m_b(Lg)$ = 0.04)

than does the somewhat flatter Shagan River test site ($m_b(P)$ - $m_b(Lg)$ = 0.27). However, Nuttli (1987) also obtained relatively low $m_b(Lg)$ for the Degelen Test Site, which is only 70 km away from Shagan River. If this Degelen-Shagan River bias is real, it is not explained by the FD results obtained to date. However, some recently archived high-quality digital seismograms recorded at the Chinese Digital Seismic Network indicate more Lg excitation (with respect to P) at Degelen than at Shagan River, which is consistent with the numerical results.

TABLE OF CONTENTS

(THIS PAGE INTENTIONALLY LEFT BLANK)

INTRODUCTION

The seismic Lg wave is one of a number of regional phases that propagate in the continental lithosphere. Because the anelastic attenuation of 1-s period Lg wave is small in shield and geologically old stable regions, Lg wave amplitudes provide a useful tool for estimating 1-s period magnitude, such as m_b for small earthquakes and explosions (Nuttli, 1973). Furthermore, the radiation of Lg is more isotropic than that of P and S waves, which adds to its usefulness as a magnitude estimator for small events, because full azimuthal coverage is not essential and thus reliable magnitude determinations can be made from the data of only a few stations (Nuttli, 1986a). Following this line, Nuttli (1986a,b, 1987, and 1988) compared m_b(P) - m_b(Lg) at the Novaya Zemlya, Nevada Test Site, the Shagan River (eastern portion of East Kazakhstan Test Site) as well as the Degelen region (central portion of East Kazakhstan Test Site) as follows:

TABLE 1. m_b(P) - m_b(Lg) AT VARIOUS SITES

Site	m_b(P) - m_b(Lg)	Reference
Novaya Zemlya	-0.11±0.02	Nuttli (1988)
Shagan River EEKTS	+0.04±0.12	Nuttli (1986b)
Degelen CEKTS	0.27±0.03	Nuttli (1987)
Nevada Test Site	-0.31±0.02	Nuttli (1986a)

The large difference between m_b(P) - m_b(Lg) values at Shagan River and Degelen, 0.23 magnitude unit, is quite surprising inasmuch as the two test sites are less than 70 km apart. Without knowing the actual values of the explosion yields at the Eastern Kazakhstan sites, it is not obvious at all to decide whether the m_b(P) or the m_b(Lg) values at Degelen are anomalous. The difference of 0.23 magnitude unit implies that, for an explosion of given yield, either the P-wave amplitudes at Degelen are 1.9 times larger than at Shagan or that the Lg-wave amplitudes are 1.9 times smaller at Degelen. Of course, both the P and Lg might be different between Degelen and Shagan for a given yield.

A number of possible explanations of the differences between m_b(P) - m_b(Lg) values at Shagan River and Degelen have been discussed (Nuttli, personal communication). The first is a difference in coupling of P and Lg waves at the two sites. Either the P-wave coupling is significantly more efficient at Degelen than at Snagan, or the Lg-wave coupling at Degelen is less than at Shagan. A second possible explanation, somewhat related to the first, is that m_b(P) is larger at Degelen because of testing practices. Station sampling bias might be considered as the third explanation, but the data Nuttli used indicate that there is little such bias, if any. A fourth explanation is related to the fact that most of the Degelen explosions are smaller than those at Shagan, and thus the reported m_b(P) values for the Degelen events might be overestimated because only stations recording large amplitude P waves were used to obtain the International Seismological Center m_b(P) values. However, Nuttli (1987) reported that the largest Degelen events of 20 February 1975, 26 March 1978, 28 July 1978, and 29 November 1978 have an average m_b(P) - m_b(Lg) value of 0.27, the same value as for the entire set of Degelen explosions. The fifth possible explanation is that the slope of m_b(Lg) versus m_b(P) is less than unity because of differences in corner frequencies in spectra.

It is the purpose of this report to check the first hypothesis. CEKTS has considerable topographic relief (Rodean, 1979) whereas EEKTS consists of folded sedimentary rocks (Nordyke, 1973). We therefore investigated several 2-D models for the excitation of SV Lg as well as P waves using linear elastic finite-difference calculations. These simplistic models simulate the excitation of far field SV and P waves from dilatational line sources embedded in 2-D heterogeneous models with and without free surface topography.

Strictly speaking, no adequate analytical theory is available to model the near-source crustal effect of the type investigated here. Lg is thought to be superpositions of higher Rayleigh and Love modes. In terms of higher modes, the complexities of mode conversions and scatter-

ing at lateral inhomogeneities are prohibitive for analytical treatment. In addition, it is not possible to tell how much energy is present in the various structures if the concept of modes has any meaning at the wavelengths involved. The problem becomes more tractable if one regards Lg as SH or SV waves trapped in the crust and having turning points above the Moho. As a crude approximation [illegible] be modeled as SH or SV waves incident on the structure to be tested at an angle such that the phase velocity is in the observed 4.2 to 4.5 km/sec range (Barker *et al.*, [illegible]; [illegible] *et al.*, 1984).

FINITE DIFFERENCE CALCULATIONS

The 2-D [illegible] popularized by Kelly *et al.* (1976) is used with the absorbing boundary conditions [illegible] and Engquist, 1977; Emerman and Stephen, 1983) on both the sides and the bottom of the grid. Free surface boundary conditions are the default on the top of the grid, since these are suitable for use in models with flat or arbitrary polygonal topography [illegible] difference code has been utilized in the modeling of effects [illegible] due to the geological structure of Yucca Valley, NTS (McLaughlin *et al.*, [illegible]) the topography at Ahaggar Plateau (McLaughlin and Jih, 1986a), as well as the [illegible] Rayleigh waves by rough topography (McLaughlin and Jih, [illegible]) and [illegible] heterogeneity (McLaughlin and Jih, 1987).

The [illegible] experiments consist of the following five types:

1. Gaussian [illegible] a 2-D white velocity field with 2-D Gaussian spatial [illegible] scatterers (i.e., mean grain size, *a*), which turns out to [illegible] correlation distance.

2. self-similar media generated by modulating the wavenumber-wavenumber spectra of a white velocity field with the 2-D Fourier transform, $\frac{a^2}{1 + k^2a^2}$, of a special Von Karmon correlation function.

3. folded layers of sinusoidal shape with specified wavelength, amplitude and velocity profile

4. dipping sedimentary layers with specified velocity profile.

5. simple layered models.

On some of the models there was superimposed fairly rough topography generated by a Markov chain. Fourteen 2-D geologic structures were used to calculate the excitation of far-field SV and P waves from dilational line sources. Some typical simplistic models are shown in Figures 1 and 2. Similar random media have been used widely in modeling the scattering or propagation of either acoustic or elastic waves by the finite-difference method (Frankel and Clayton, 1984, 1986; Levander and Hill, 1985; Levander, 1985; Frankel and Wennerberg, 1987; McLaughlin and Jih, 1987). In the heterogeneous portion of the grid, the S-wave velocity (β) was assumed to be directly related to the P-wave velocity (α) by the following linear relationship: for $\alpha < 2.8$, $\beta = 0.45\ \alpha$; for $3.2 < \alpha < 4.8$, $\beta = 0.50\ \alpha$; for $\alpha > 5.2$, $\beta = 0.59\ \alpha$; and linear interpolation was used for the transition intervals. These heterogeneous media are then embedded into a homogeneous half space with P- and S-wave velocities of 6 and 3.55 km/sec respectively.

The incident wave is a broadband Ohnaka planar SV wave with apparent velocities of 4.5 km/sec incident upon these models. The dilational strain was recorded at an array of locations with an average depth of 0.5 km in the grid. By use of the reciprocity principle, the displacement response at far distance (teleseismic) was determined for a dilational line source with a

von Seggern and Blandford (1972) reduced displacement potential for 50KT in hard rock. The same technique has been utilized previously in modeling the effects of the geologic structure of Yucca Valley (McLaughlin *et al.*, 1987) as well as that of the topographic configuration of Ahaggar mountain on teleseismic $m_b(P)$ (McLaughlin and Jih, 1986). One minor difference is that here the incidence angles of the incoming SV- and P wave were 52° and 20° respectively, corresponding to the appropriate apparent velocity range. To assure that the initial incoming wave lies completely in the homogeneous half space, we have selected grid dimensions of 250 by 430 and 250 by 250 for SV- and P wave simulations, respectively. The mesh spacings were $\Delta x = \Delta z = 0.050$km. Thus the two grids are of the same width 12.5km and two different depths: 21.5km and 12.5km. Due to the limitation of the grid size, the heterogeneous crustal layers were set to 2 or 3 km. This distinction with the realistic crustal depth should be kept in mind when interpreting the results. Although the temporal spacing was 0.005 sec, the band beyond 5 Hz is less reliable due to the inevitable grid dispersion of finite-difference simulation.

The FD synthetics were deconvolved/convolved so as to represent the outgoing waves due to the same explosion line source in each model. The results from these simulations are presented in Table 2. The excitation of P- and SV- waves for each model are referenced to the excitation for a uniform 2 km layer (α = 5.0km/s, β = 2.74km/s) over a uniform half space (α = 6.0km/s, β = 3.55km/s). The models are arranged in order of decreasing SV Lg excitation relative to the reference model (j=0). Data shown under columns P and Lg are $\log(P_j/P_0)$ and $\log(Lg_j/Lg_0)$ respectively, where both P and Lg are the averaged peak amplitude measurement of the synthetics derived from deconvolution, low pass filtering etc.

TABLE 2. COMPARISON OF EXPLOSION P AND SV Lg EXCITATION

model	P	Lg	P-Lg	Description of the model
0	0.000	0.000	0.000	1-uniform layer (5+0%, 2km thick)
1	-0.207	0.202	-0.409	rough TOPO + 1 uniform layer (5+0%, 2km thick)
2	-0.006	0.132	-0.139	gentle TOPO + self-similar layer (5+10%, 2km)
3	-0.196	0.110	-0.305	rough TOPO + Gaussian layer (5+10%, 2km)
4	-0.023	0.073	-0.096	gentle TOPO + 1 uniform layer (5+0%, 2km)
5	-0.034	0.044	-0.078	self-similar layer (5+10%, 2km thick)
6	-0.162	0.019	-0.181	folded sinusoidal layers(L=2,H=2.5,5+20%)
7	-0.031	0.014	-0.045	folded sinusoidal layers(L=2,H=2.5,5+10%)
8	-0.134	-0.037	-0.098	self-similar layer (5+20%, 2km thick)
9	-0.029	-0.037	0.008	folded sinusoidal layers(L=5,H=2.5,5+10%)
10	0.003	-0.058	0.061	2-Gaussian layer (4.5+10%/5+10%, total 2km)
11	0.019	-0.091	0.110	steeply dipping layers (52^o)
12	0.011	-0.093	0.104	gently dipping layers (26^o)
13	0.018	-0.137	0.155	steeply dipping layers (-52^o)
14	0.009	-0.143	0.152	gently dipping layers (-26^o)

Some observations are immediate:

1. For self-similar models, weak variation in the medium velocities causes more Lg generation.

2. Dipping layers (models 11 through 14) generate smaller Lg than the normalizing model.

3. Media with topography (e.g. models 1 through 4) which represent CEKTS all generate more Lg than the normalizing model.

4. Dipping layers (models 11 through 14) are more efficient than all other models for P excitation.

5. m_b(P) - m_b(Lg) at EEKTS (e.g. models 11 through 14) are larger than for any other model.

We have noticed that the smoothing of the interface between the sediment layer and the half space would not significantly affect the result.

Observations 2,3,4 and 5 can be explained easily as that topography creates more apparent explosion P-SV(Lg) coupling. The introduction of interfaces alone does not of itself increase SV excitation with the required slowness range. Although this result is in seeming contradiction to Nuttli's (1987) CEKTS-EEKTS observation, our previous numerical experiments tend to support this explanation.

As a comparison, the results corresponding to frequency-domain measurements are also presented for the 0.5-1.0 Hz bandwidth in Table 3. Again, the average spectral level of the dilatational strain history in the 0.5-1.0 Hz bandwidth from the array of locations is determined relative to a reference model. Note that the results under the Lg and P-Lg columns in Table 3 follow the same pattern as the time-domain approach with the exception of the folded models and the 20% self-similar model.

TABLE 3. EXPLOSION EXCITED P AND SV Lg ON 0.5-1.0 Hz

model	P	Lg	P-Lg	*Description of the model*
0	0.000	0.000	0.000	reference model
1	-0.400	0.083	-0.483	rough TOPO+uniform layer(5+0%,2km)
2	-0.049	0.057	-0.106	gentle TOPO+self-similar layer(5+10%,2km)
3	-0.363	0.063	-0.426	rough TOPO+Gaussian layer(5.0+10%,2km)
4	-0.180	0.019	-0.199	gentle TOPO+uniform layer(5+0%,2km)
5	0.016	0.009	0.007	self-similar layer(5+10%,2km)
6	0.099	-0.031	0.130	folded sinusoidal layers(5+20%,L=2,H=2.5)
7	0.058	-0.101	0.159	folded sinusoidal layers(5+10%,L=2,H=2.5)
8	-0.026	-0.049	0.023	self-similar layer(5+20%,2km)
9	0.015	-0.163	0.178	folded sinusoidal layers(5+10%,L=5,H=2.5)
10	0.083	-0.007	0.090	2-Gaussian layer(4.5+10%/5.0+10%,2km)
11	-0.008	-0.048	0.040	steeply dipping layers(52^o)
12	-0.024	-0.057	0.033	gently dipping layers(26^o)
13	0.015	-0.086	0.101	steeply dipping layers(-52^o)
14	-0.001	-0.103	0.102	gently dipping layers(-26^o)

DISCUSSIONS AND CONCLUSIONS

The method of finite-difference was used to simulate the excitation of explosion generated far-field P and SV Lg waves in various models of crustal heterogeneity. While we continue to experiment with various models, our preliminary results indicate that P to SV conversion is strongly enhanced by velocity variation in the vicinity of rough topography and the introduction of low velocity layers near the surface. The introduction of interfaces alone does not of itself increase SV excitation with the required slowness range.

These synthetic results are consistent with observations for Novaya Zemlya (Nuttli, 1988) and Shagan River (Nuttli,1986), based on WWSSN film chip readings of Lg. The Novaya Zemlya, which has rough topography, has a higher Lg relative to P ($m_b(P) - m_b(Lg) = 0.04$) than does the somewhat flatter Shagan River test site ($m_b(P) - m_b(Lg) = 0.27$). However, Nuttli (1987) also obtained relatively low $m_b(Lg)$ for the Degelen Test Site, which is only 70 km away from Shagan River. If this Degelen-Shagan River bias is real, it is not explained by the FD results obtained to date. However, some recently archived high-quality digital seismograms recorded at the Chinese Digital Seismic Network indicate more Lg excitation (with respect to P) at Degelen than at Shagan River, which is consistent with our numerical results (Figure 41).

Although we cannot presently explain Nuttli's (1987) Degelen results, we predict substantial variations in SV Lg excitation by explosions embedded in crustal heterogeneity. It seems that P-to-SV is not the only mechanism for explosion Lg excitation, so it is necessary to investigate the excitation of SH(Lg) as well.

A possibility is that Nuttli's m_b:Lg relationship might be related to Rayleigh-to-P conversion away from the immediate location of the source. Our numerical simulations treated only the P-S conversions that might occur within a few km of the source, and given some simple

models. If either the Rayleigh excitation or the Rayleigh scattering is different for CEKTS and EEKTS, then we could see the difference in Rayleigh to Lg. Since the two locations are only 70 km apart, the Rayleigh-to-Lg difference would presumably have to occur in the first 20-25 seconds. Thus it seems necessary to examine if the P-coda are different for Degelen and Shagan in the first 20-25 seconds. Similarly, P-SV conversion could be happening further away from the source than we are modeling. It is also possible that the non-linear source effects might produce larger SV at one site versus another. These hypothesis as well as the 3-dimensional effects were not addressed in our current experiments.

Baumgardt (personal communication, 1987) pointed out that the observations at NORSAR for Degelen and Shagan events (Ringdal, 1982) did not show the bias, and he proposed another explanation for Nuttli's observations as that Nuttli's Degelen observations were made almost entirely with stations to the south, whereas the Shagan data contain observations from the NW at Scandinavian stations. His station corrections for Q may therefore have been biased. Baumgardt (1985) proposed that Lg loses energy as it crosses the Urals on its way to the Scandinavian stations, and this loss may not be accounted for in Nuttli's Q. It is interesting to note that in Nuttli's (1986b) original paper on Shagan events, his revised Q_0 values are the same as or less than the original Q_0 values for all the Scandinavian stations. The reduced Q_0 values resulted because the Scandinavian m_b(Lg) values were less than average.

The finite-difference results in Figures 39 and 40 also show negatively correlated P and SV energy. This provides a preliminary explanation of the success of the unified yield estimator (U.S. Congress, Office of Technology Assessment, 1988). It seems that measuring all possible phases reduces the effects of uneven energy release on source size estimation. To understand this issue in a more quantitative manner, and to derive an optimal weighting scheme to combine all phases, theoretical studies with numerical simulations are necessary.

ACKNOWLEDGMENTS

We wish we could thank Otto Nuttli in person for partly motivating this research. This work was supported by DARPA contract F19628-86-C-0054, monitored by the Air Force Geophysics Laboratory. The views and conclusions contained in this work are those of the authors and should not be interpreted as necessarily representing the official policies, either expressed or implied, of the Defense Advanced Research Projects Agency or the U.S. Government.

McLaughlin, K. L. and R.-S. Jih (1986a), Scattering from near-source topography: teleseismic observations and numerical 2-D explosive line source simulations, Section III of *Report AFGL-TR-86-0159 (TGAL-86-03)* Teledyne Geotech, Alexandria, VA (ADA 183013).

McLaughlin, K. L. and R.-S. Jih (1986b), Finite-difference simulations of Rayleigh wave scattering by 2-D rough topography, *Report AFGL-TR-86-0269 (TGAL-86-09)*, Teledyne Geotech, Alexandria, VA (ADA 179190).

McLaughlin, K. L. and R.-S. Jih (1987), Finite-difference simulations of Rayleigh wave scattering by shallow heterogeneity, *Report AFGL-TR-87-0322 (TGAL-87-02)*, Teledyne Geotech, Alexandria, VA (available through NTIS).

Nordyke, M. D. (1973), A review of Soviet data on the peaceful uses of nuclear explosions, *Report UCRL-51414*, Lawrence Livermore Laboratory, University of California, CA (available through NTIS).

Nuttli, O. W. (1986a), Yield estimates of Nevada Test Site explosions obtained from seismic Lg waves, *J. Geophys. res.*, **91**, 2137-2151.

Nuttli, O. W. (1986b), Lg magnitudes of selected East Kazakhstan underground explosions, *Bull. Seism. Soc. Am.*, **76**, 1241-1251.

Nuttli, O. W. (1987), Lg magnitudes of Degelen, East Kazakhstan, underground explosions, *Bull. Seism. Soc. Am.*, **77**, 679-681.

Nuttli, O. W. (1988), Lg magnitudes and yield estimates for underground Novaya Zemlya nuclear explosions, *Bull. Seism. Soc. Am.*, **78**, 873-884.

Ringdal (1983), Magnitude from P coda and Lg using NORSAR data, in *Scientific Report No.2-82/83, NORSAR Semiannual Technical Summary, 1 Oct 82 - 31 Mar 83*, Linda B. Tronrud (ed.), 72-80 (available through NTIS).

Rodean, H. C. (1979), ISC events from 1964 to 1976 at and near the nuclear testing ground in eastern Kazakhstan, *Report UCRL-52856*, Lawrence Livermore Laboratory, University of California, CA (available through NTIS).

U.S. Congress, Office of Technology Assessment (1988), Seismic verification of nuclear testing treaties, *OTA-ISC-361*, U.S. Government Printing Office, Washington, DC.

GENERAL REFERENCES

Der, Z. A., M. E. Marshall, A. O'Donnell, T. W. McElfresh (1984), Spatial coherence structure and attenuation of the Lg phase, site effects, and the interpretation of the Lg coda, *Bull. Seism. Soc. Am.*, **74**, 1125-1147.

Der, Z. A., T. W. McElfresh, R. Wagner, and J. Burnetti (1985), Errata to "Spectral characteristics of P waves from nuclear explosions and yield estimation" *Bull. Seism. Soc. Am.*, **75**, 1222.

Der, Z. A., C. P. Mrazek, E. Smart, and B. W. Barker (1978), Some aspects of Lg and Pg propagation, *Report SDAC-TR-78-11*, Seismic Data Analysis Center, Teledyne Geotech, Alexandria, VA (available through NTIS).

Der, Z. A., A. O'Donnell, T. W. McElfresh, R. Juula, J. A. Burnetti, M. Marshall, M. Silk and F. Gordon (1982), A study of seismic wave propagation at regional distances in five areas of the world, *Report VSC-TR-82-14*, Seismic Data Analysis Center, Teledyne Geotech, Alexandria, VA (available through NTIS).

Der, Z. A., A. O'Donnell, P. J. Klouda (1981), As investigation of attenuation, scattering and site effects on regional phases, *Report VSC-TR-81-11*, Seismic Data Analysis Center, Teledyne Geotech, Alexandria, VA (available through NTIS).

Herrmann, R. B. (1987), Lg wave excitation and propagation in the presence of one-, two-, and three-dimensional heterogeneities, *Report AFGL-TR-87-0229*, St. Louis Univ., St. Louis, MO (available through NTIS).

Teledyne Geotech (1980), Studies of seismic wave characteristics at regional distances, *Report AL-80-1*, Teledyne Geotech, Alexandria, VA (available through NTIS).

FIGURE CAPTIONS

Figure 1. Typical geological models used in the finite-difference simulations in this report, which included: (A) model 5: a 2 km thick self-similar layer of mean α = 5 km/sec and 10% variation, superimposed on a homogeneous half space with α = 6 km/sec. (B) A 2 km thick Gaussian layer of mean α = 5 km/sec and 10% variation, mean grain size = 1 km. (C) model 7: a 3 km thick sedimentary rock of folded layers with sinusoidal shape. The folded layers have wavelength 2 km, peak-to-peak amplitude 2.5 km. Each layer is uniform in material property, and the profile of α is Gaussian distributed with mean 5 km/sec, ν = 10%. The interface between the half space and the folded layers is smoothed. (D) model 9: similar to (C) except that the folded layers have wavelength 5 km.

Figure 2. (E) model 3: a rough topography superimposed on a 2 km thick Gaussian layer. (F) Same as (E) except that the layer is uniform with α = 5 km/sec. (G) model 2: similar to (E), except for self-similar velocity variation and different topography. (H) model 4: same as (G) except for uniform layer. The rough topography was generated by a Markov chain with larger transition probability, which yielded "more frequent" small-scale elevation changes.

Figure 3. Model 2. P wave in a half space (α = 6.0 km/s, β = 3.55 km/s) incident upon a 2 km layer with average P-wave velocity of 5 km/s and a self-similar 10% rms velocity variation superimposed by a gentle topography (indicated in the 0 sec frame). The S-wave velocity is assumed to be proportional to the P-wave velocity. Darkness of the snapshots are proportional to the displacement amplitude. Snapshots of the displacement field are shown at 1 second intervals. The dilatational strain is recorded at 32 locations at a depth of 0.5 km in order to infer the excitation of far-field P waves from explosion sources. Although absorbing boundary conditions are used, care must be taken to avoid residual reflections from the sides of the grid.

Figure 4. Model 7. Same as Figure 3 except that a 3 km thick sedimentary rock of folded layers with sinusoidal shape. The folded layers have wavelength 2 km, peak-to-peak amplitude 2.5 km. Each layer is uniform in material property, and the profile of α is Gaussian distributed with mean 5 km/sec, ν = 10%. The interface between the half space and the folded layers is smoothed (see Figure 1 (C)).

Figure 5. Model 8. Same as Figure 3 except the layer has P-wave velocity of 5 km/s and a self-similar 20% rms velocity variation (indicated in the 0 sec frame).

Figure 6. Model 14. Same as Figure 5 except that the gently dipping layers totaling 3 km thick are superimposed on the half space. The sedimentary layers have Gaussian distributed profile with mean 5 km/sec, ν = 10%.

Figure 7. Model 2. S wave in a half space (α = 6.0 km/s, β = 3.55 km/s) incident at 52^o upon a 2 km self-similar layer with average P-wave velocity of 5 km/s and 10% rms velocity variation superimposed by a gentle topography (indicated in the 0 sec frame). The dilatational strain is recorded at 32 locations at a depth of 0.5 km in order to infer the excitation of far-field S waves from explosion sources.

Figure 8. Model 5. Same as Figure 7 except that the self-similar layer is flat(indicated in the 0 sec frame).

Figure 9. Model 9. Same as Figure 7 except that the 3 km thick low velocity layer consists of lightly folded (5 km wavelength, 2.5 km amplitude) 0.5 km thick layers with 10% rms velocity variation with respect to an average velocity of 5 km/s.

Figure 10 Model 14. Same as Figure 7 except that the half space is superimposed by gently dipping layers totaling 3 km thick. The sedimentary layers have Gaussian distributed profile with mean 5 km/sec, ν = 10%.

Figure 11. Model 1. Synthetic far-field P- (top) and SV-wave (bottom) inferred by the principle of reciprocity. The original dilatational strain history (5 Hz low-pass) responding to incident broadband P or SV plane wave recorded at 32 locations at 0.5 km depth in the reference model. Shown here are the deconvolved synthetics corresponding to VSB 50 KT in hard rock. The peak amplitude of these synthetics was measured and compared to the average peak amplitude of the reference model.

Figure 12. Same as Figure 11 except for model 2.

Figure 13. Same as Figure 11 except for model 3.

Figure 14. Same as Figure 11 except for model 4.

Figure 15. Same as Figure 11 except for model 5.

Figure 16. Same as Figure 11 except for model 6.

Figure 17. Same as Figure 11 except for model 7.

Figure 18. Same as Figure 11 except for model 8.

Figure 19. Same as Figure 11 except for model 9.

Figure 20. Same as Figure 11 except for model 10.

Figure 21. Same as Figure 11 except for model 11.

Figure 22. Same as Figure 11 except for model 12.

Figure 23. Same as Figure 11 except for model 13.

Figure 24. Same as Figure 11 except for model 14.

Figure 25. Average spectral ratio as a function of frequency, $Log(\frac{P_1}{P_0})$ (upper) and $Log(\frac{Lg_1}{Lg_0})$ (lower), of the Model 1 relative to the reference model. P wave response of model 1 in the 0.5 to 1.0 Hz range is deficient with respect to the reference model by 0.348 log units, while the S wave response is 0.063 log unit above the reference model. Vertical bars represent the standard error of a single observation.

Figure 26. Same as Figure 25 except for model 2.

Figure 27. Same as Figure 25 except for model 3.

Figure 28. Same as Figure 25 except for model 4.

Figure 29. Same as Figure 25 except for model 5.

Figure 30. Same as Figure 25 except for model 6.

Figure 31. Same as Figure 25 except for model 7.

Figure 32. Same as Figure 25 except for model 8.

Figure 33. Same as Figure 25 except for model 9.

Figure 34. Same as Figure 25 except for model 10.

Figure 35. Same as Figure 25 except for model 11.

Figure 36. Same as Figure 25 except for model 12.

Figure 37. Same as Figure 25 except for model 13.

Figure 38. Same as Figure 25 except for model 14.

Figure 39. Averaged P and SV(Lg) peak amplitudes of array of shallow explosions in fourteen crustal models sorted with the $\log_{10}(Lg/Lg_0)$ values. Several observations are obvious: (1) Dipping layers (models 11 through 14) generate smaller Lg than the normalizing model, while they all generate more P than the reference model. (2) Media with topography (e.g. models 1 through 4) which represent CEKTS all generate more Lg than the normalizing model, while they excite less P due to strong P to S conversion. (3) Dipping layers (models 11 through 14) are more efficient than all other models for P excitation. Thus $m_b(P)$ and $m_b(Lg)$ appear to be negatively correlated.

Figure 40. Same as Figure 39 except the P and SV(Lg) excitations are measured with the averaged spectral content in [0.5,1] Hz band. Crustal models with topography generate more Lg and less P than models with dipping layers, same as the result derived from peak amplitude measurement.

Figure 41. Short period seismograms of two Shagan events 87171 (78.74E, 49.91N, mb=6.1) and 87347 (78.85E, 49.96N, mb=6.1), and a Degelen event 87198 (78.11E, 49.80N, mb=5.8) recorded at CDSN station WMQ. Each trace is scaled by the peak amplitude. Note the relatively less P energy (with respect to Lg energy) in the Degelen event 87198 as compared to Shagan events of similar magnitudes.

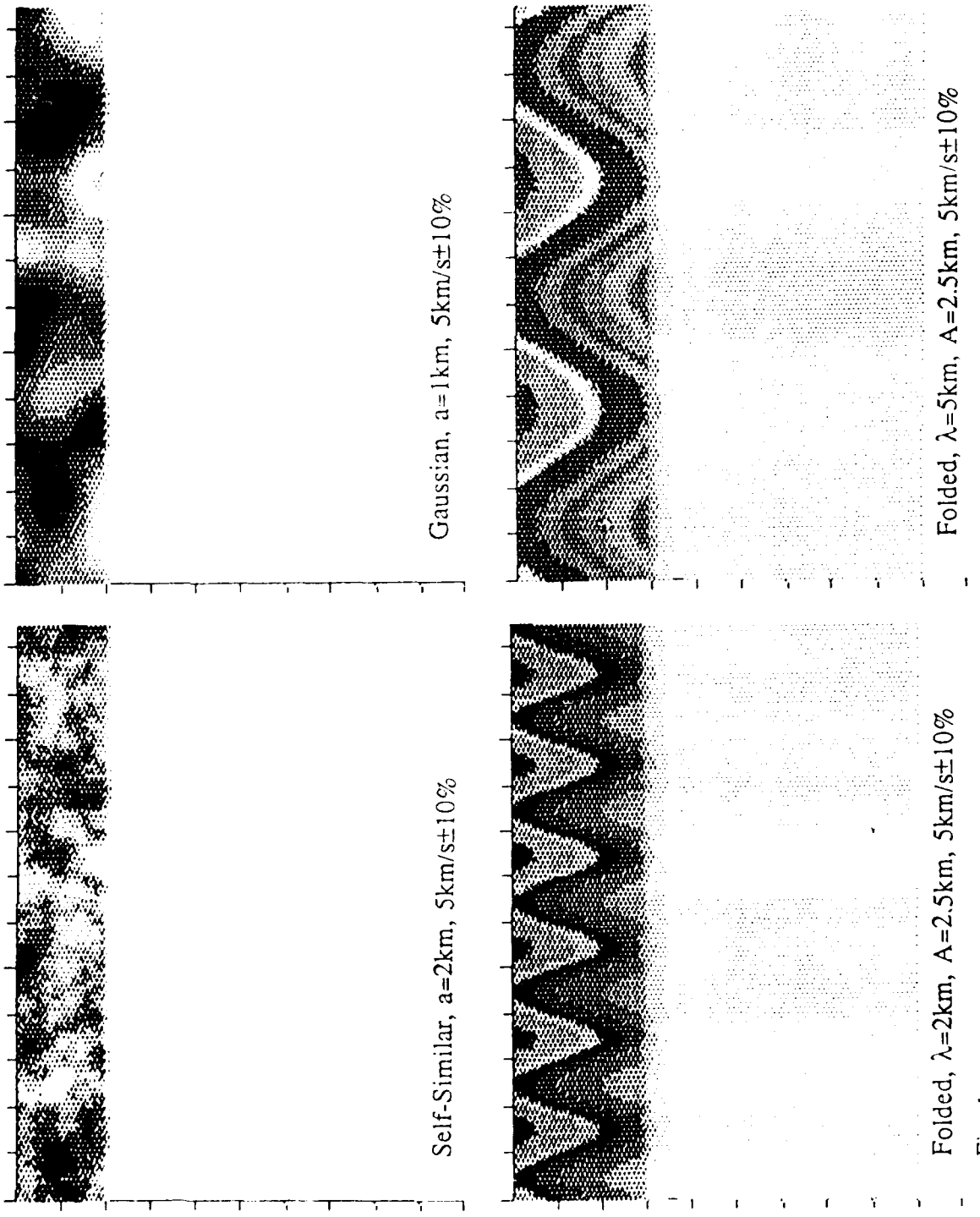
Gaussian, a=1km, 5km/s±10%
Folded, λ=5km, A=2.5km, 5km/s±10%
Self-Similar, a=2km, 5km/s±10%
Folded, λ=2km, A=2.5km, 5km/s±10%

Fig. 1

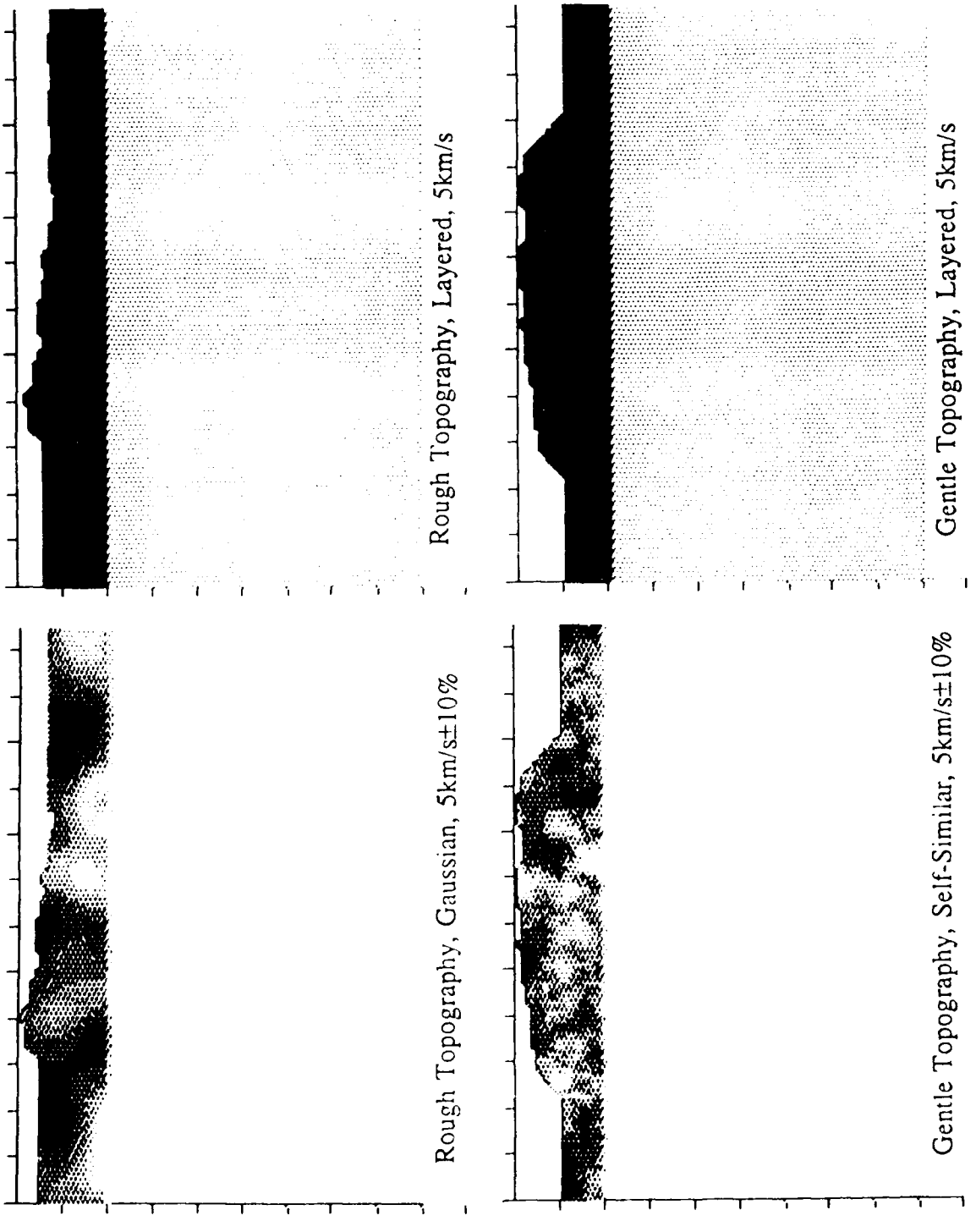
Rough Topography, Layered, 5km/s
Gentle Topography, Layered, 5km/s
Rough Topography, Gaussian, 5km/s±10%
Gentle Topography, Self-Similar, 5km/s±10%

Fig. 2

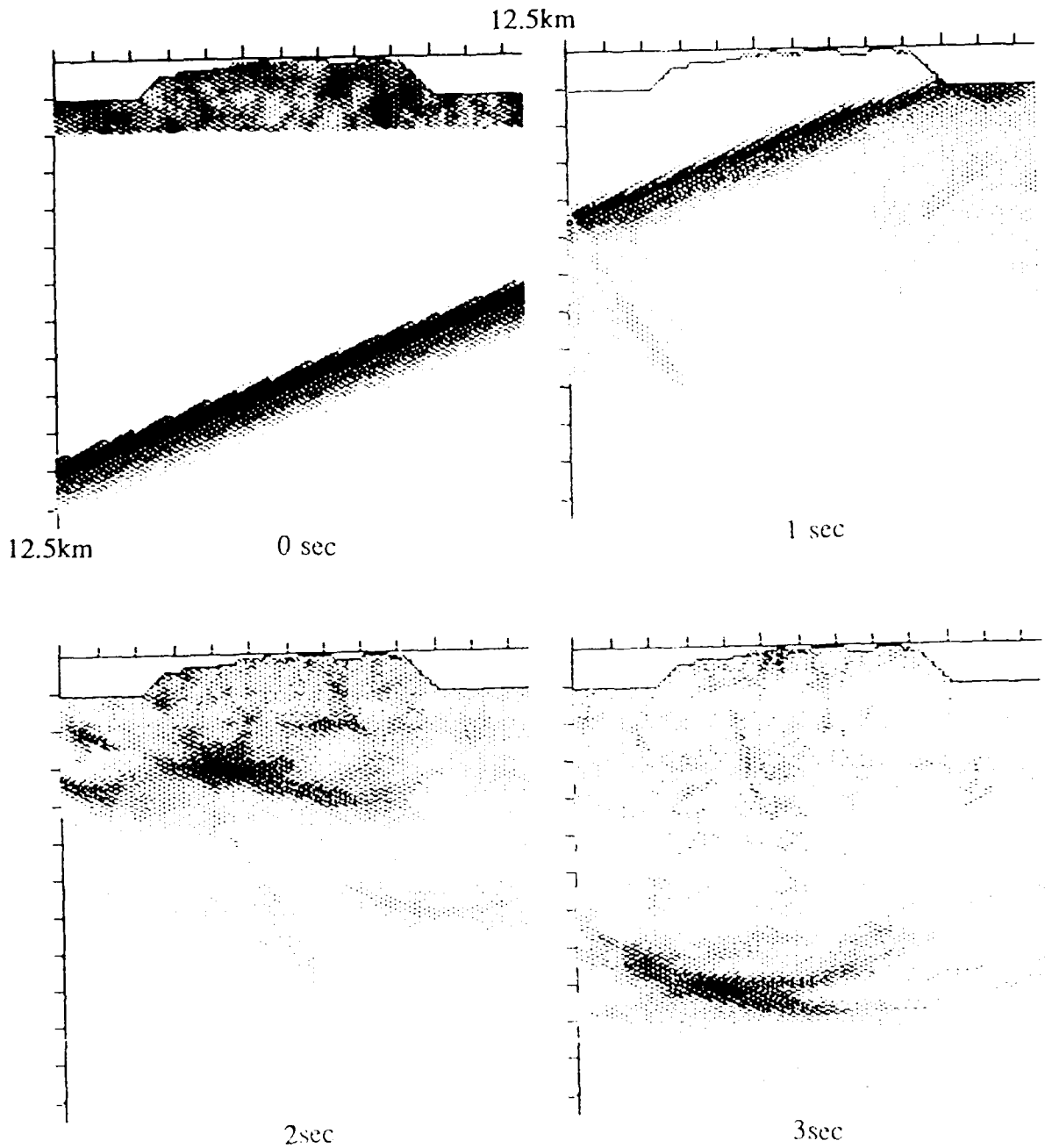

P wave, 20°

Self-Similar Model with Gentle Topography, 5km/s±10%

Fig. 3

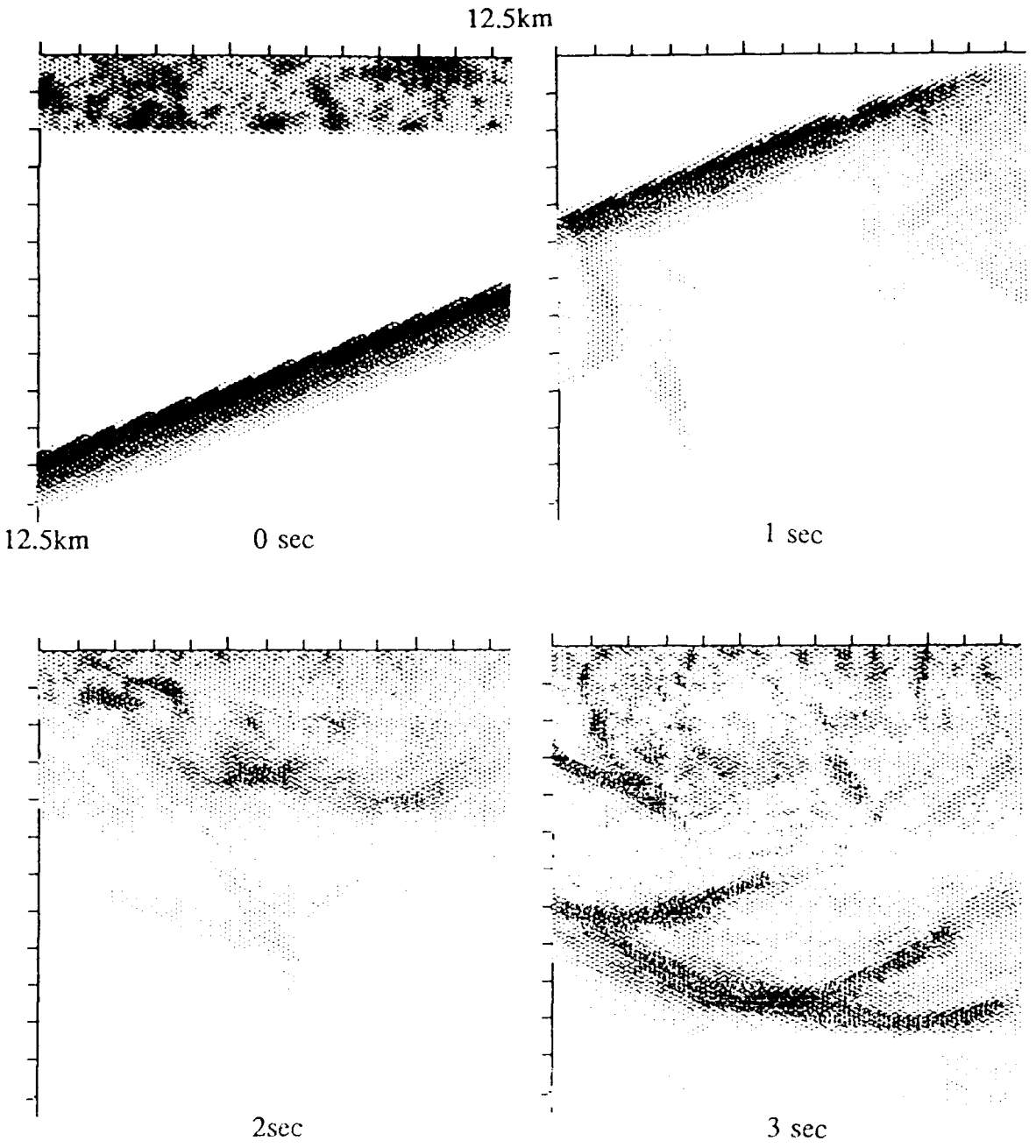

P wave, 20°

Self-Similar Model, a=2km, 5km/s±20%

Fig. 4

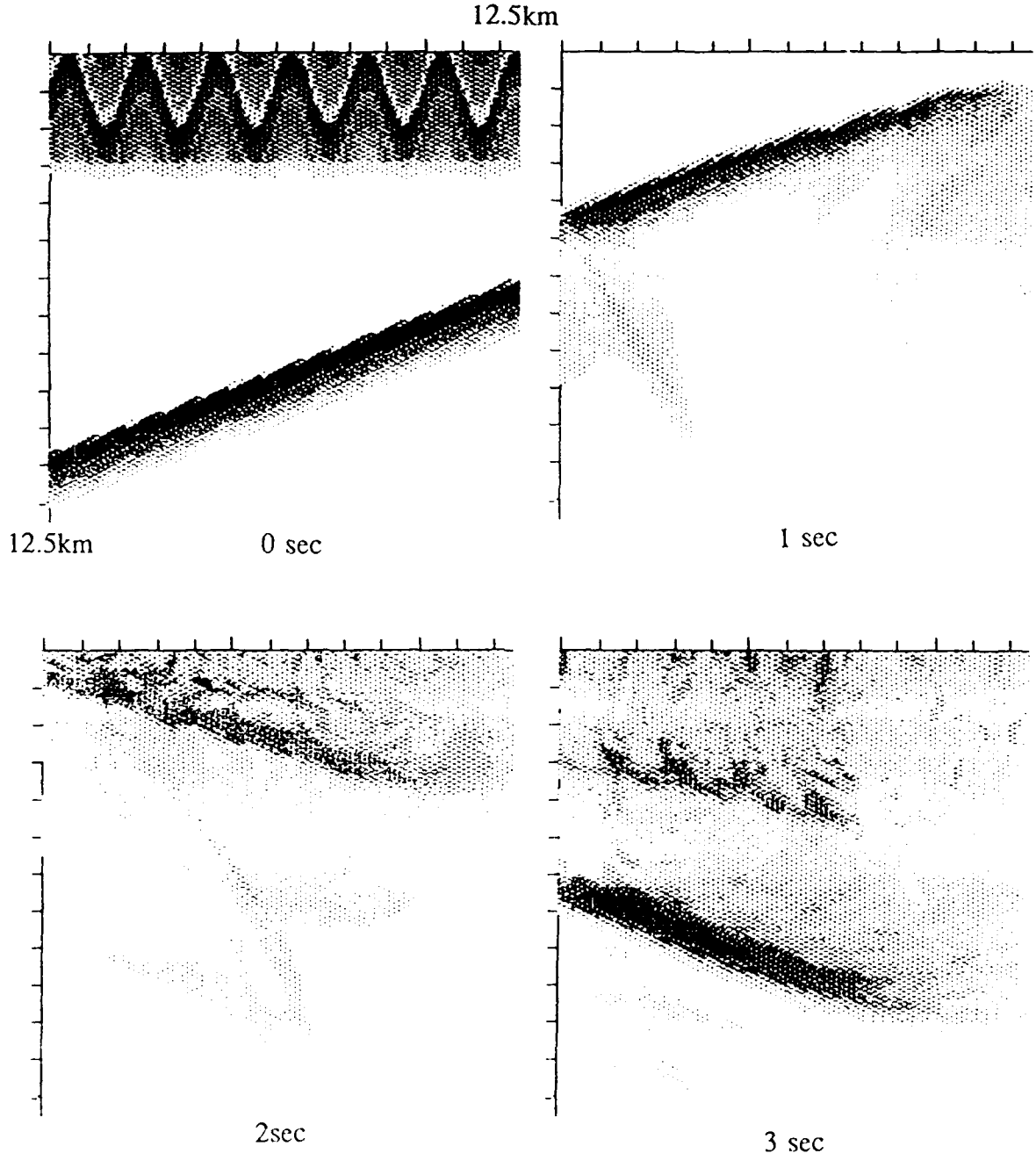

P wave, 20°

Folded Model, λ=3km, A=2.5km, 5km/s±10%

Fig. 5

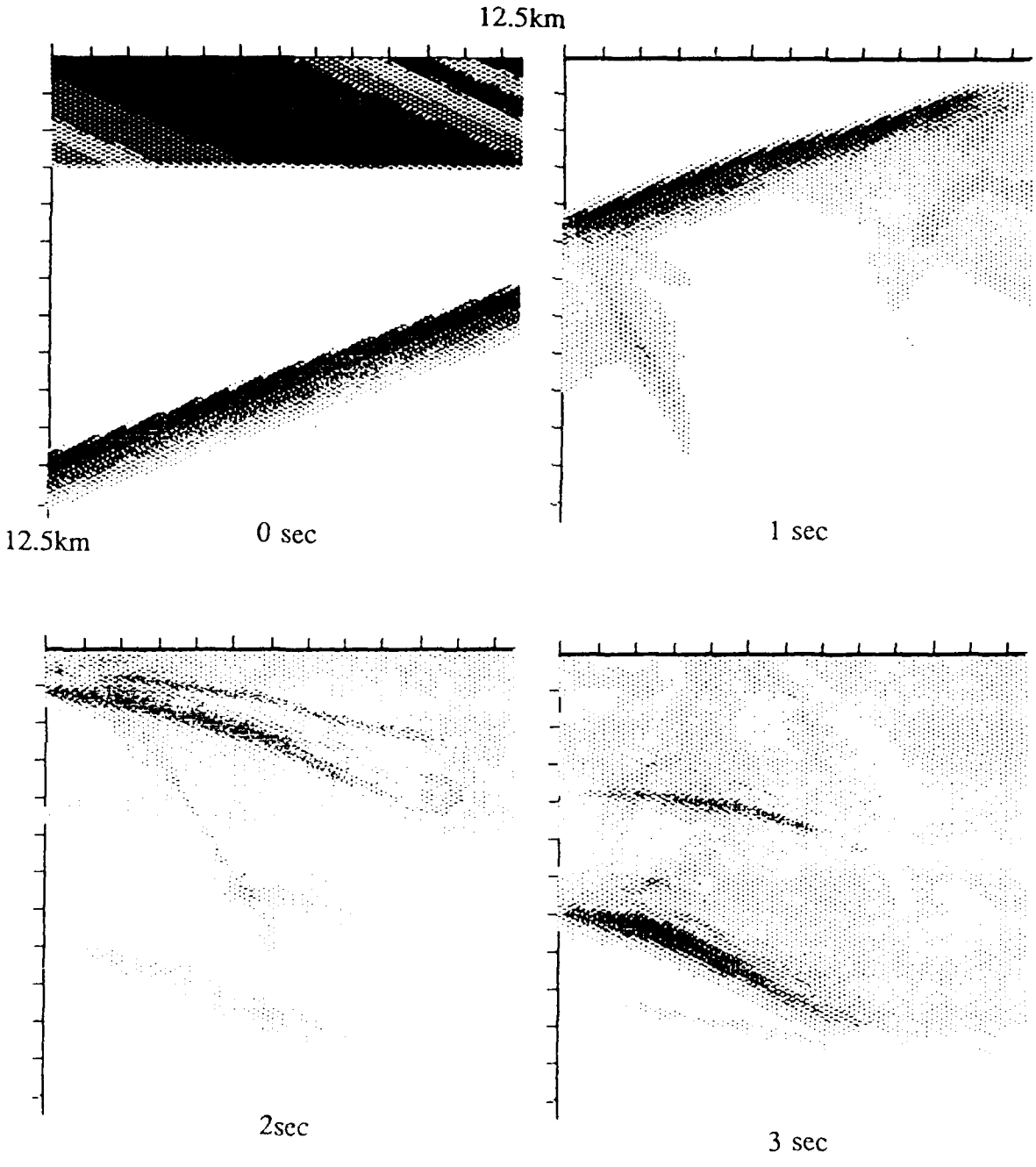

P wave, 20°

Gently Dipping Model, 5km/s±10%, –26°

Fig. 6

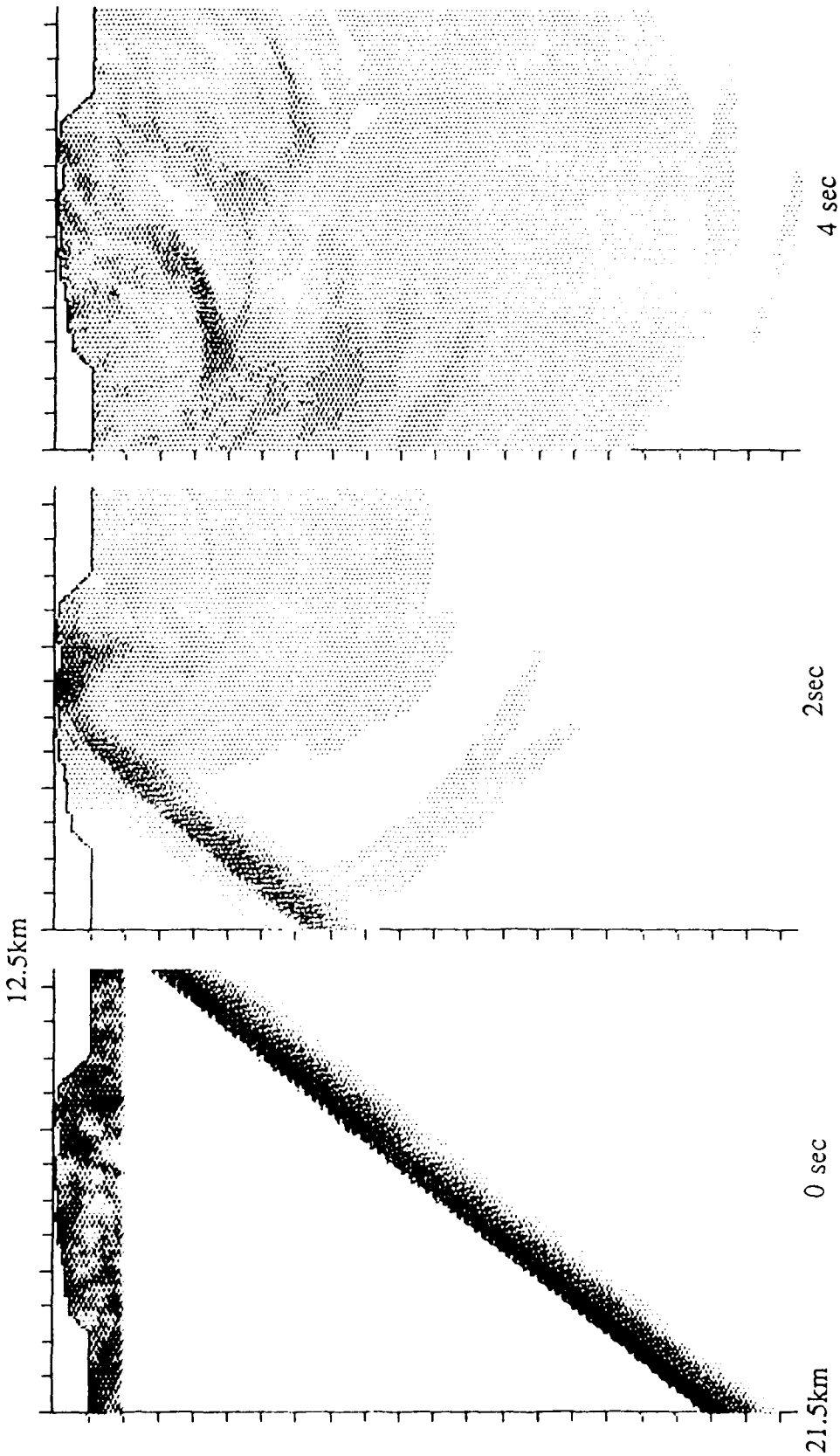

Self-Similar Model with Gentle Topography, 5km/s±10%

Fig. 7

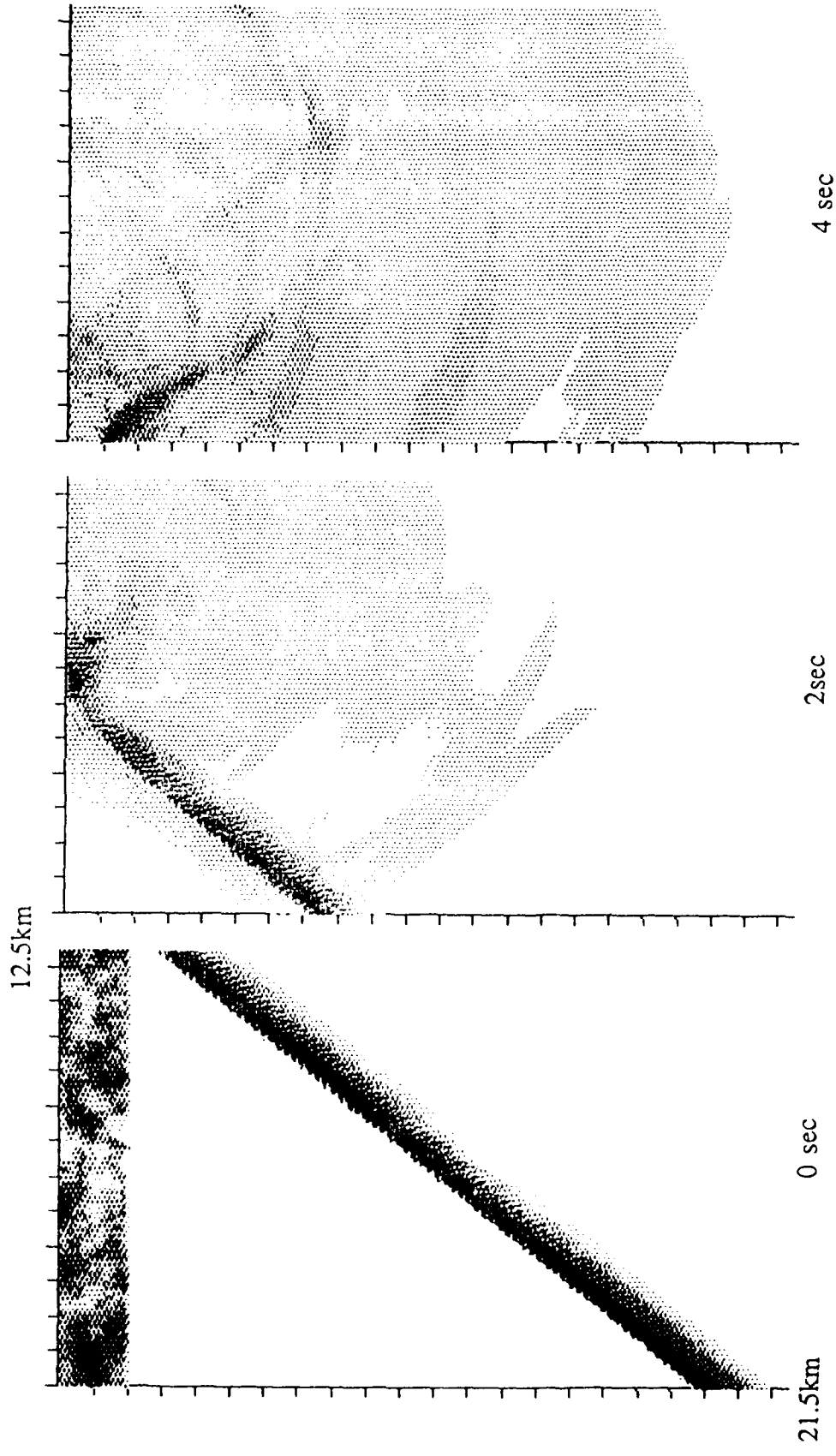
4 sec
SV wave, 52°
2sec
12.5km
0 sec
21.5km
Self-Similar Model, a=2km, 5km/s±10%

Fig. 8

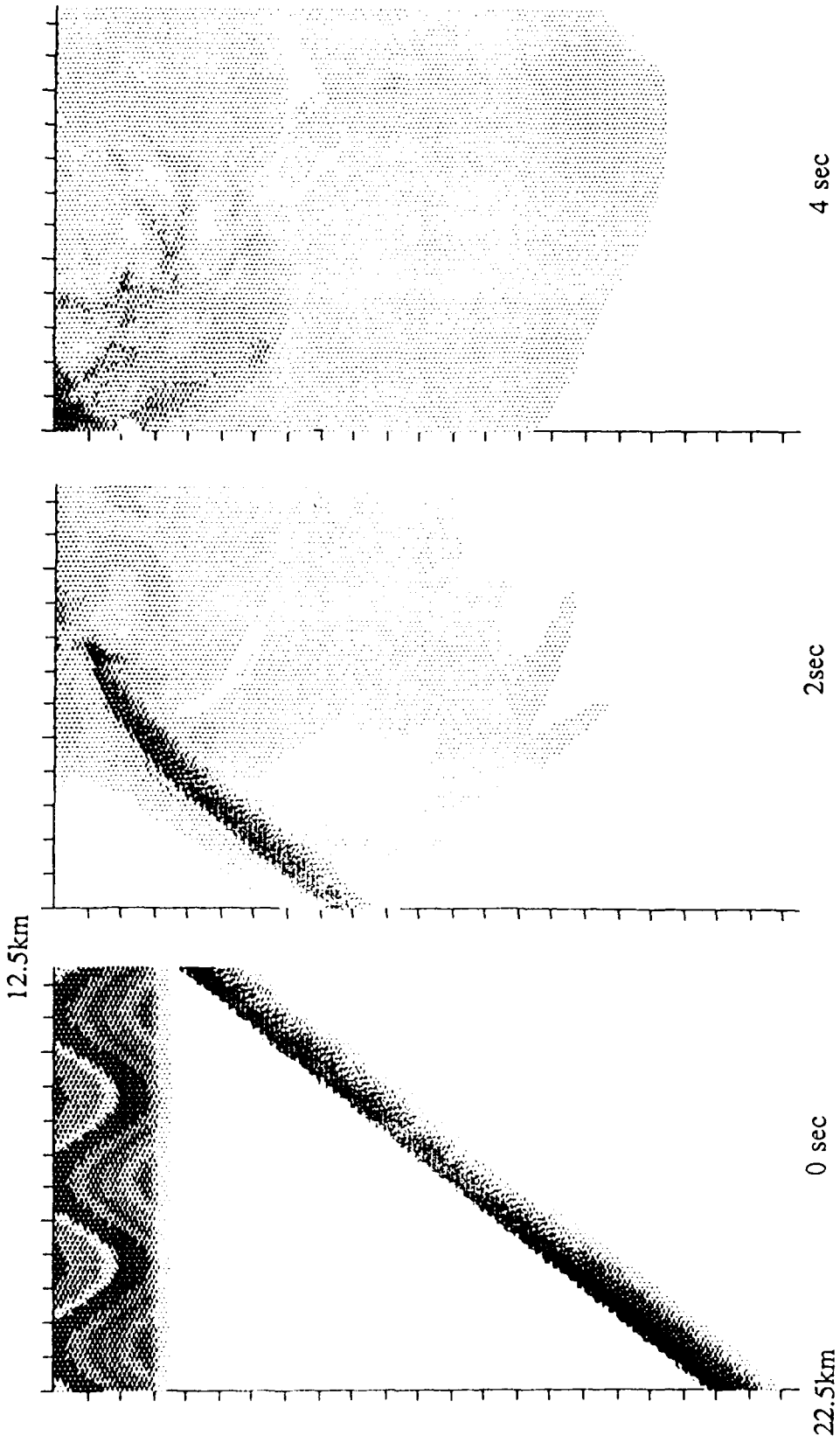
4 sec
2sec
0 sec
12.5km
22.5km
SV wave, 52°
Folded Model, λ=5km, A=2.5km, 5km/s±10%

Fig. 9

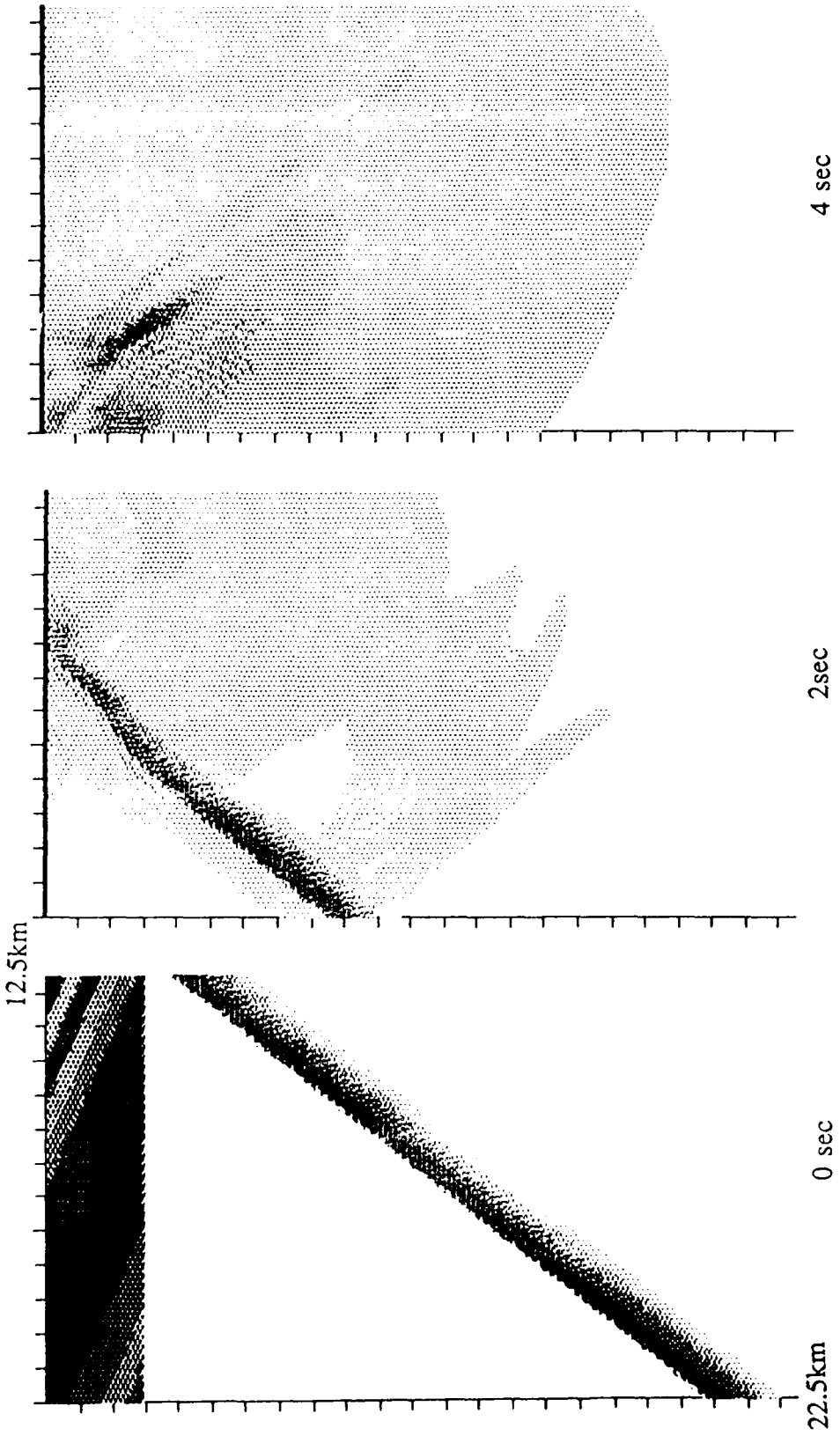
4 sec
SV wave, 52°
2sec
12.5km
0 sec
22.5km
Gently Dipping Model, 5km/s±10%, −26°

Fig. 10

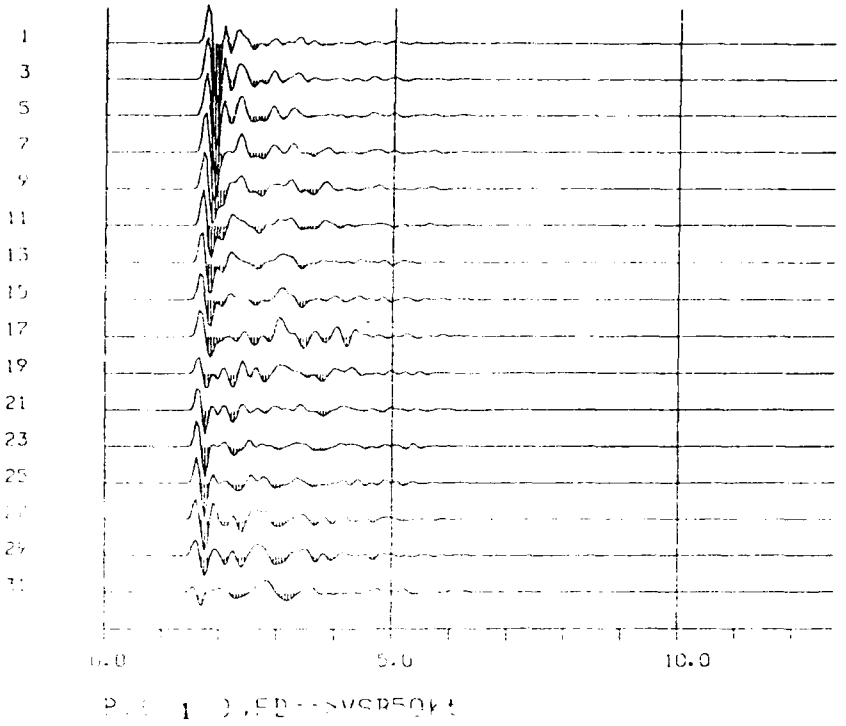
1
3
5
7
9
11
13
15
17
19
21
23
25
27
29
31
5.0
10.0

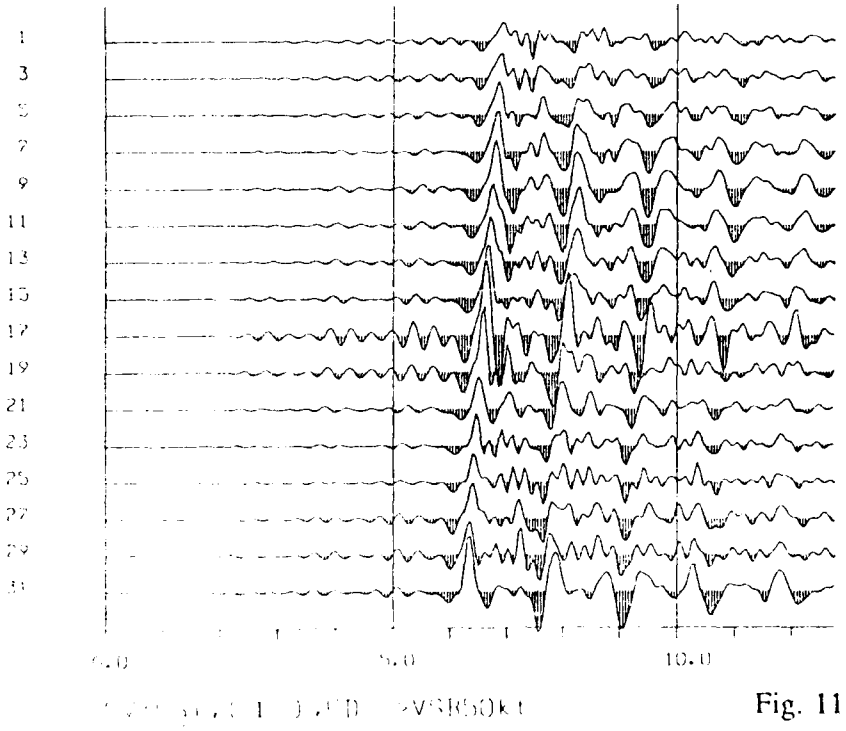
1
3
5
7
9
11
13
15
17
19
21
23
25
27
29
31
5.0
10.0

Fig. 11

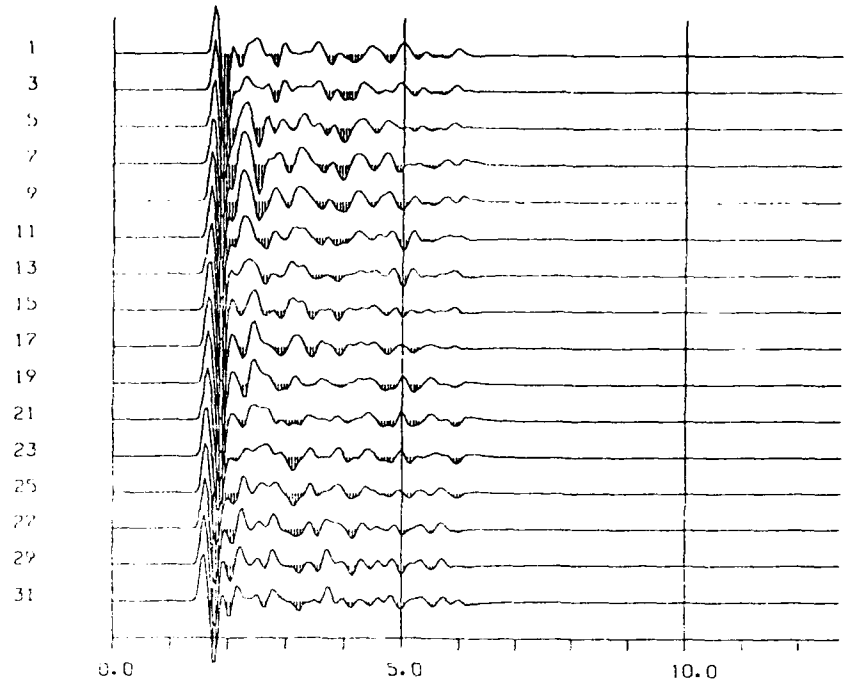
1
3
5
7
9
11
13
15
17
19
21
23
25
27
29
31
0.0
5.0
10.0
P, 2 ,FD==>VSB50kt

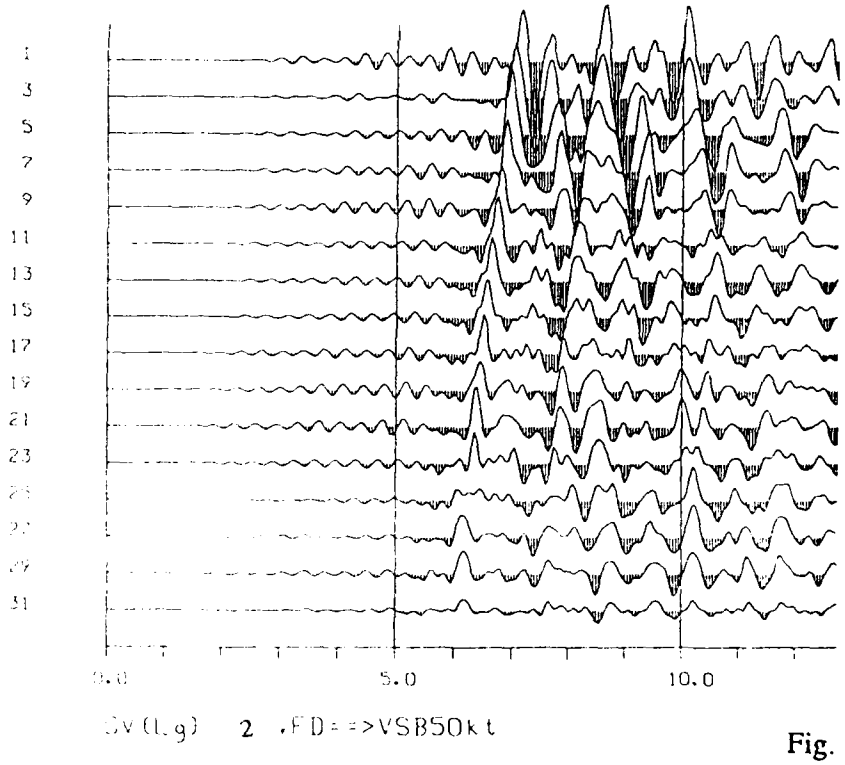
1
3
5
7
9
11
13
15
17
19
21
23
25
27
29
31
0.0
5.0
10.0
SV(Lg) 2 ,FD==>VSB50kt

Fig. 12

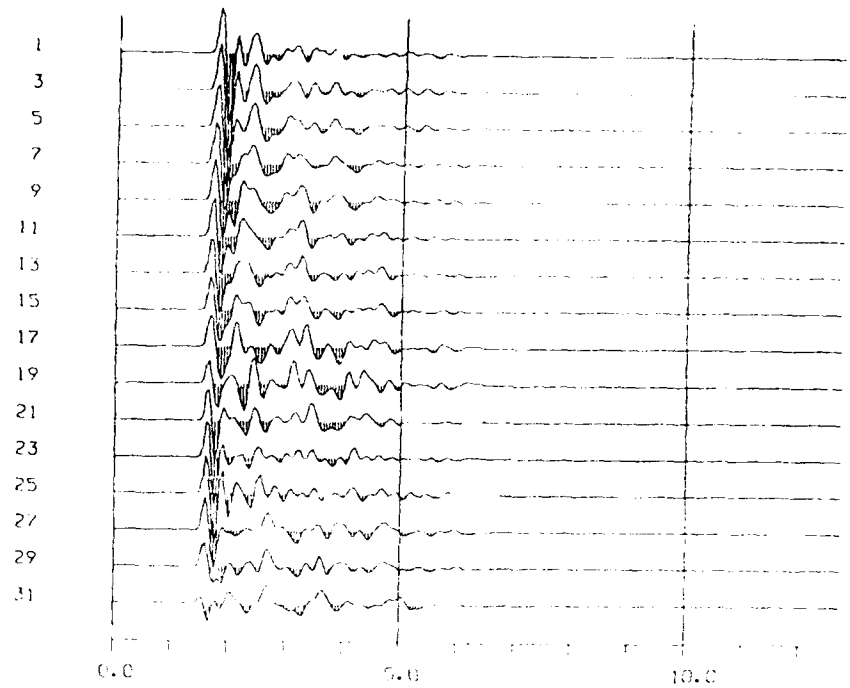
1
3
5
7
9
11
13
15
17
19
21
23
25
27
29
31
0.0
5.0
10.0

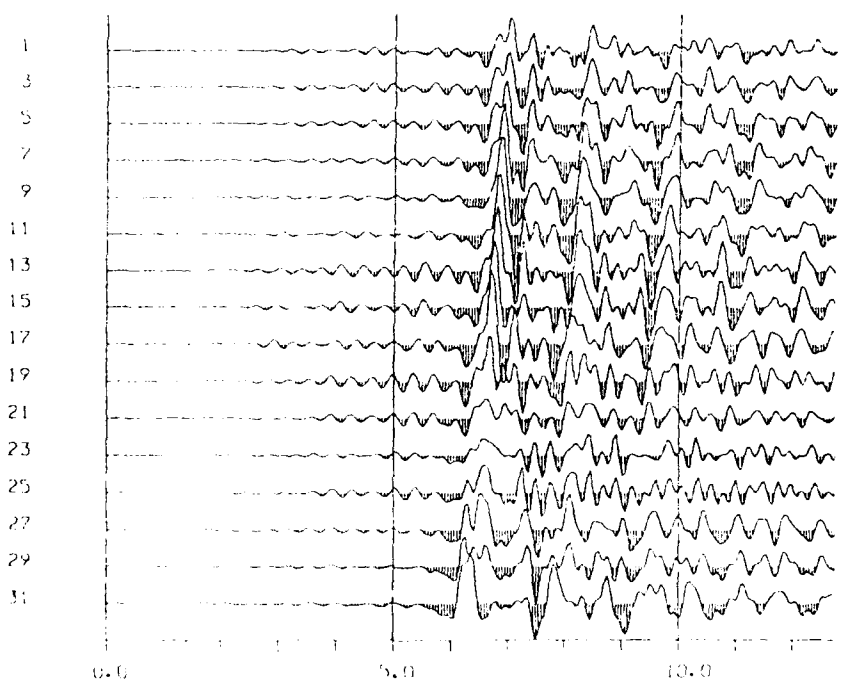
1
3
5
7
9
11
13
15
17
19
21
23
25
27
29
31
0.0
5.0
10.0

Fig. 13

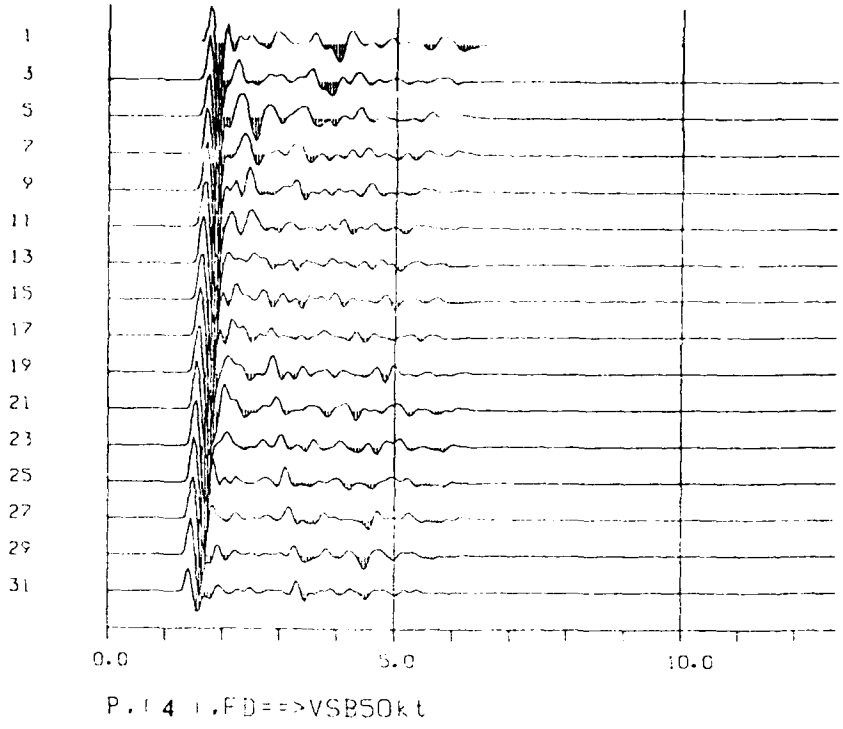
1
3
5
7
9
11
13
15
17
19
21
23
25
27
29
31
0.0
5.0
10.0
P, 4 , FD=>VSBSOkt

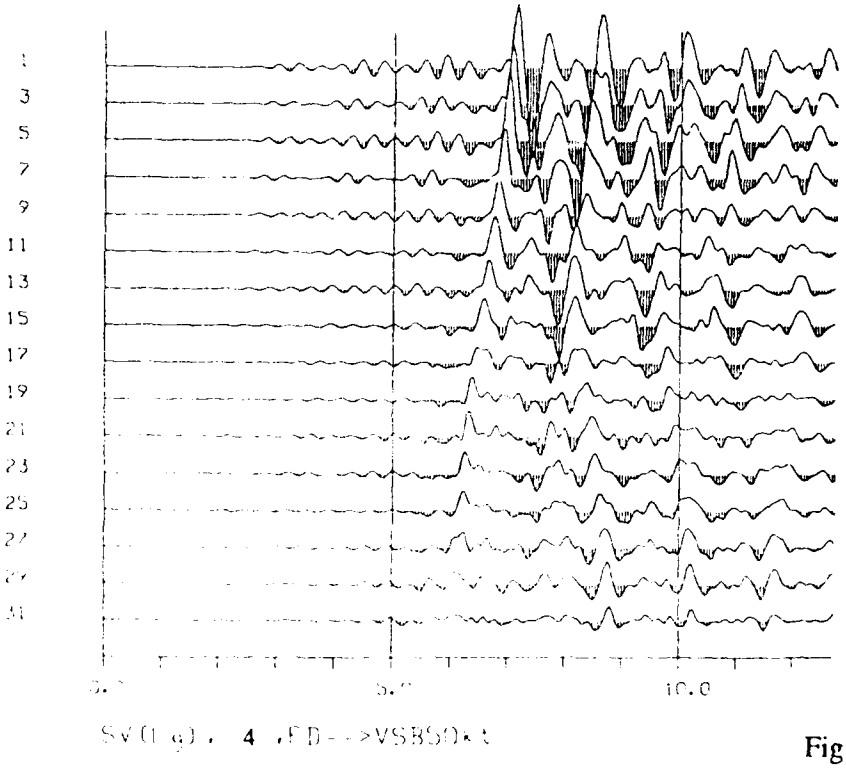
1
3
5
7
9
11
13
15
17
19
21
23
25
27
29
31
10.0
SV(Lg), 4 , FD=>VSBSOkt

Fig. 14

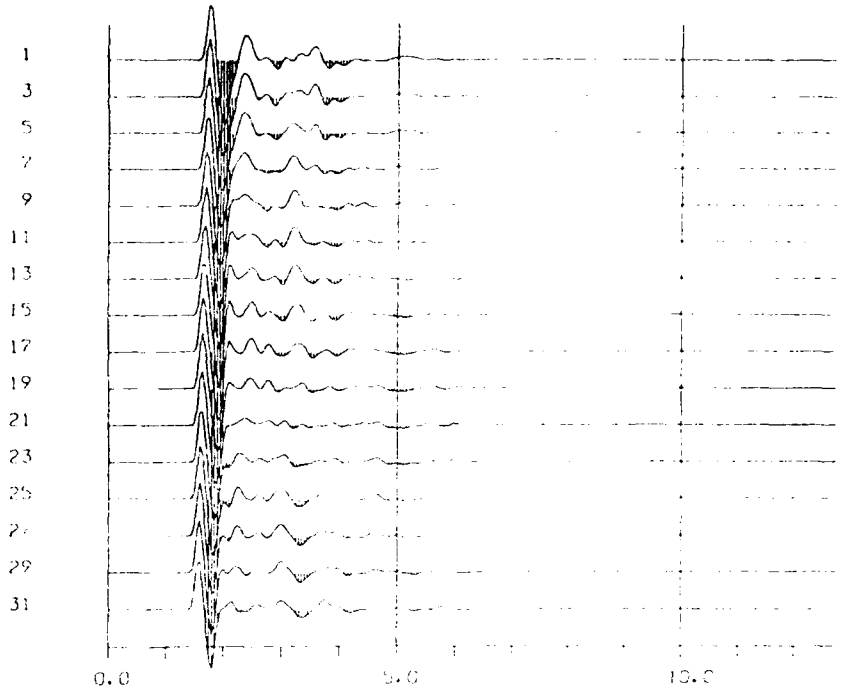

P,(5),FD==>VSB50kt

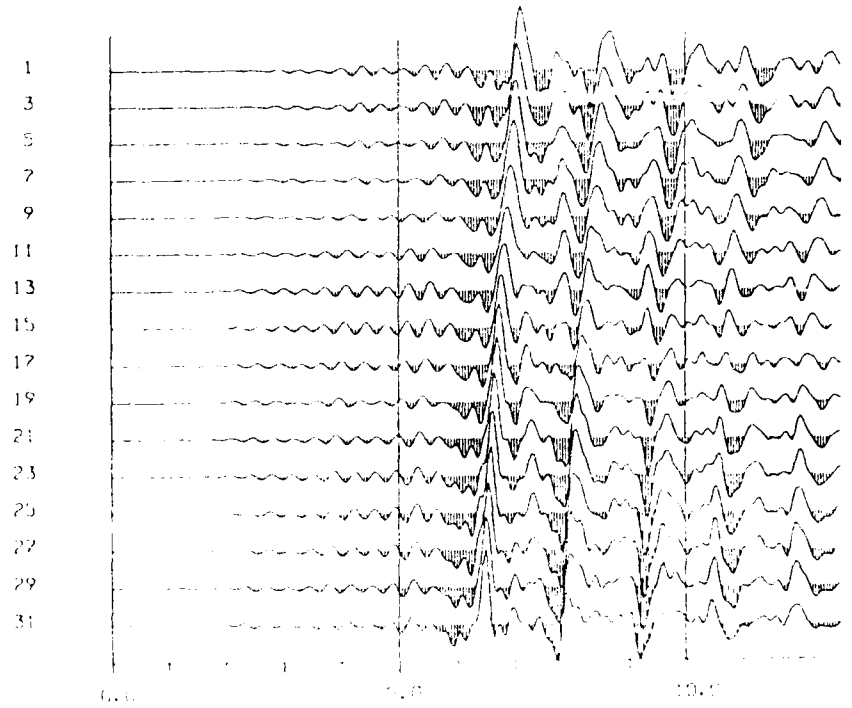

SV(Lg),(5),FD ==>VSB50kt

Fig. 15

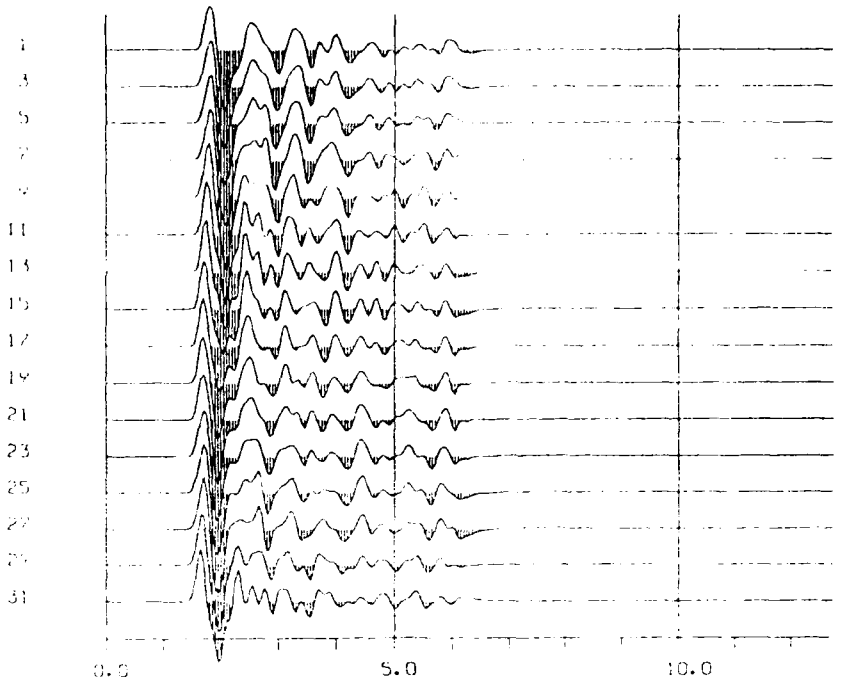

P, 6 ,FD=>VSB50kt

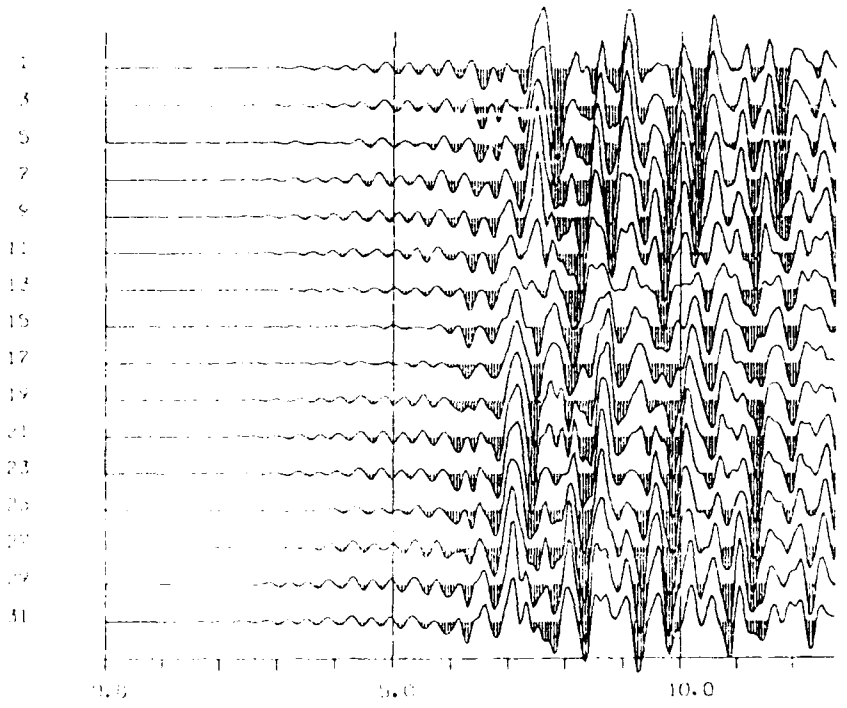

SV(Lg) 6 ,FD=>VSB50kt

Fig. 16

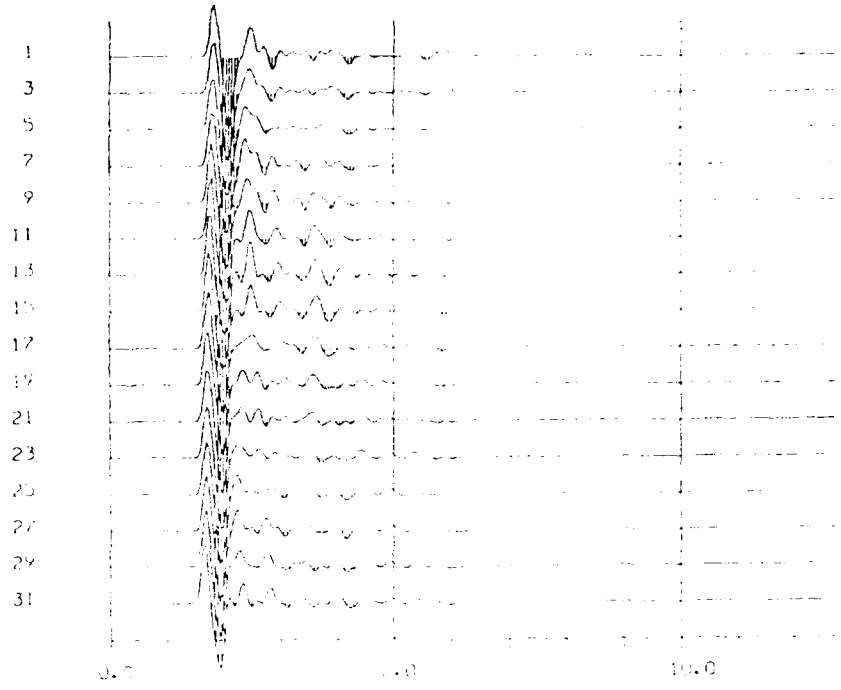
1
3
5
7
9
11
13
15
17
19
21
23
25
27
29
31

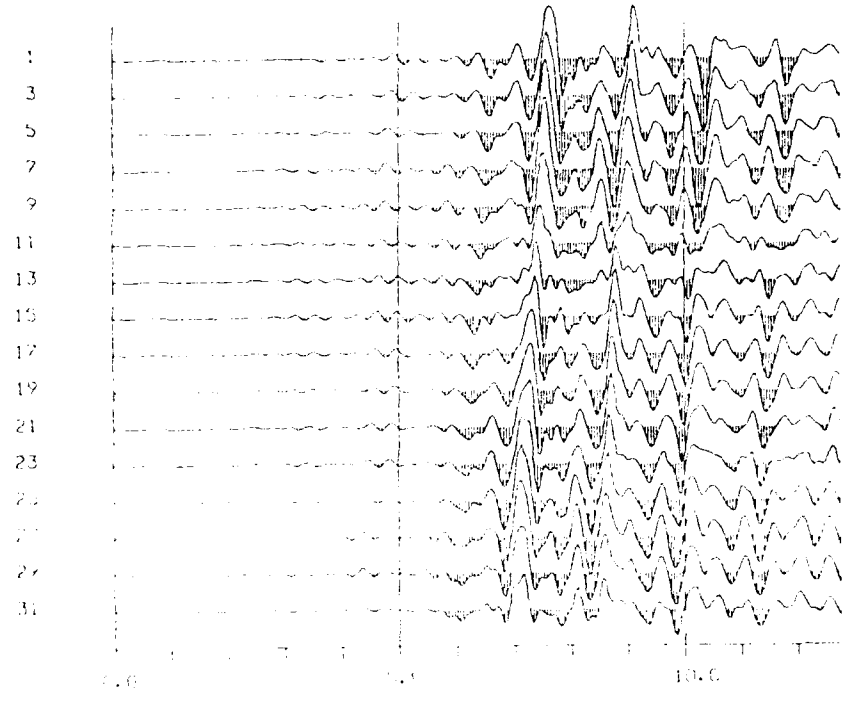
1
3
5
7
9
11
13
15
17
19
21
23
25
27
29
31

Fig. 17

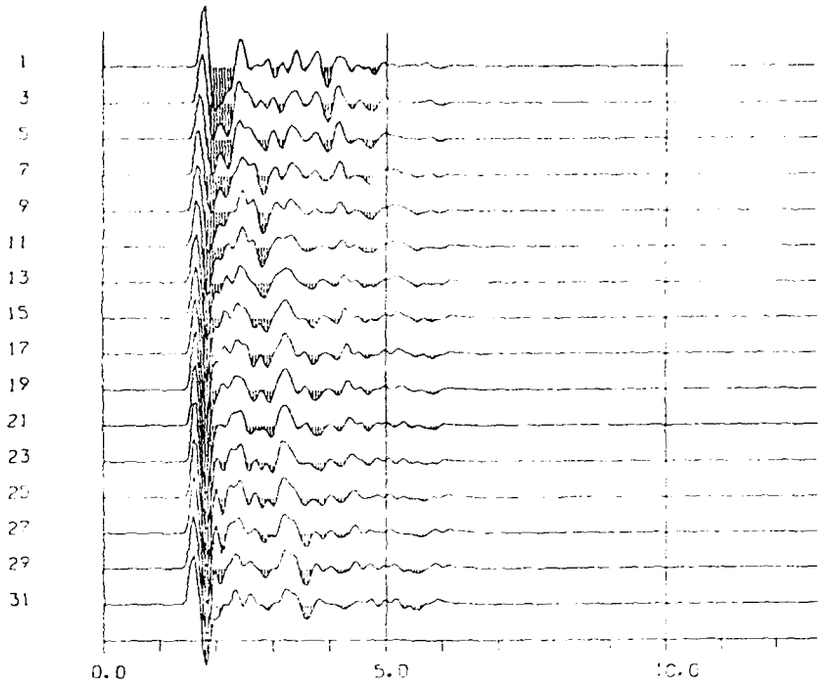
1
3
5
7
9
11
13
15
17
19
21
23
25
27
29
31
0.0
5.0
10.0
P, (8) ,FD==>VSB50kt

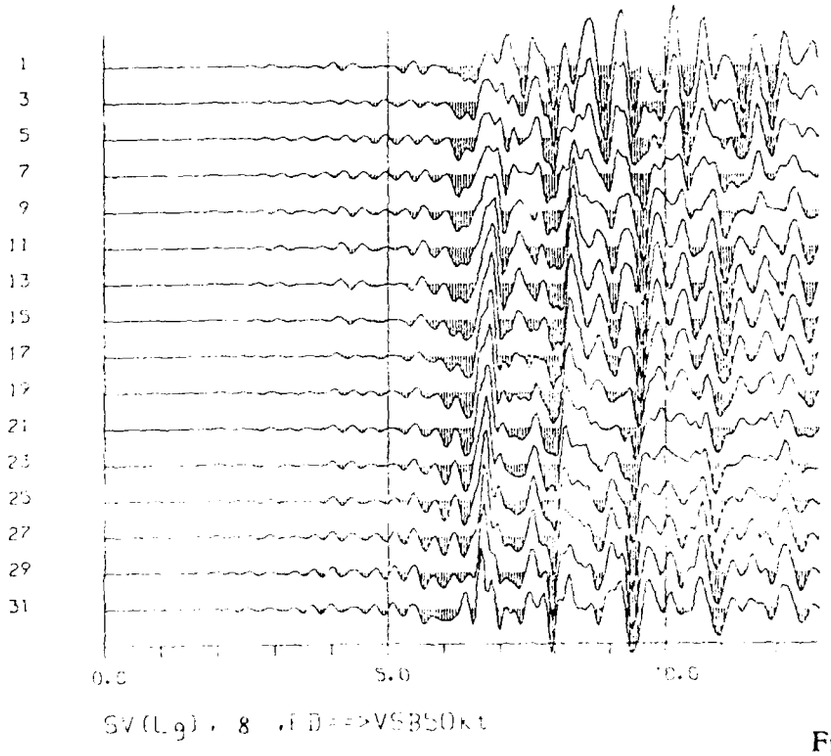
1
3
5
7
9
11
13
15
17
19
21
23
25
27
29
31
0.0
5.0
10.0
SV(Lg) , 8 ,FD==>VSB50kt

Fig. 18

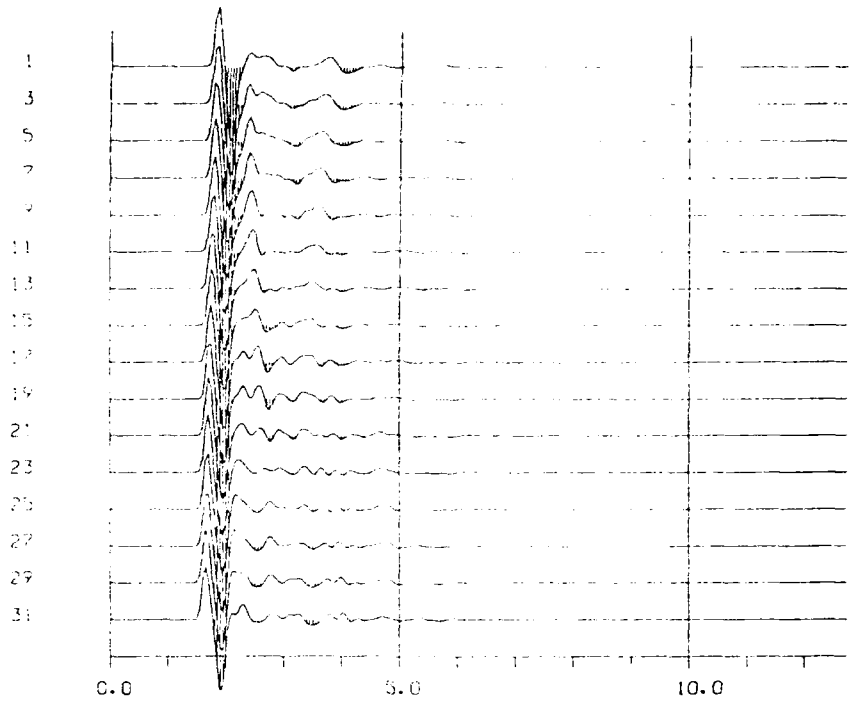
1
3
5
7
9
11
13
15
17
19
21
23
25
27
29
31
0.0
5.0
10.0
P,(9),FD==>VSB50kt

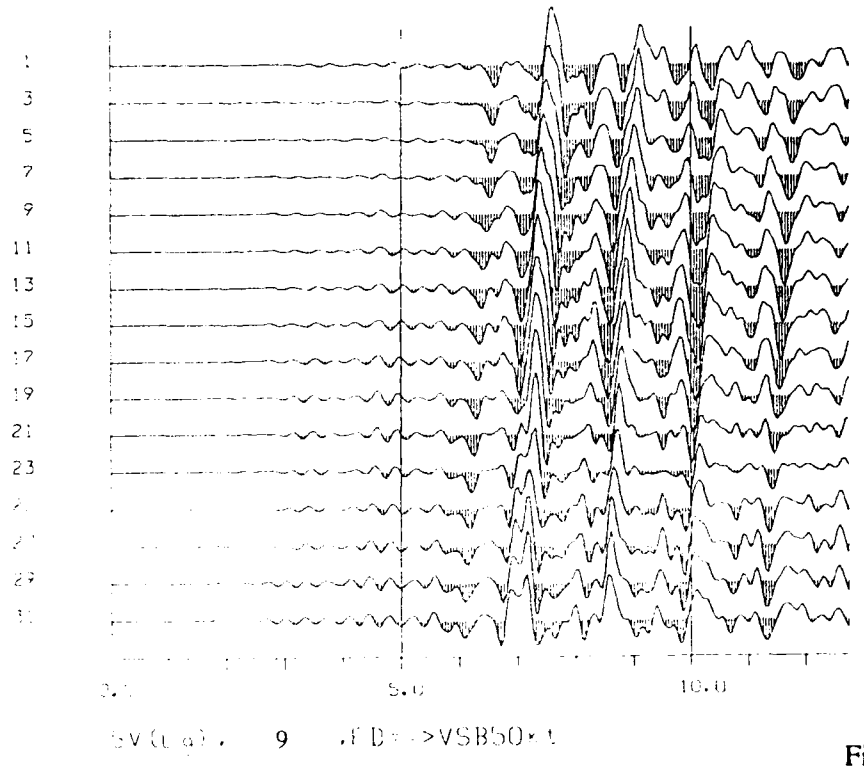
1
3
5
7
9
11
13
15
17
19
21
23
25
27
29
31
5.0
10.0

Fig. 19

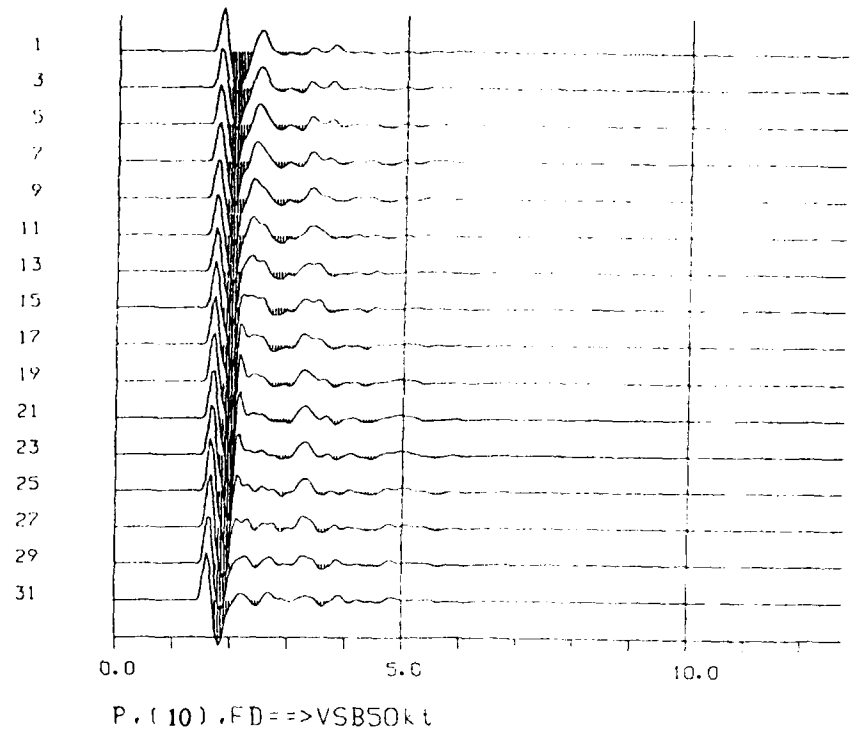
1
3
5
7
9
11
13
15
17
19
21
23
25
27
29
31
0.0
5.0
10.0
P, (10) , FD= =>VSB50kt

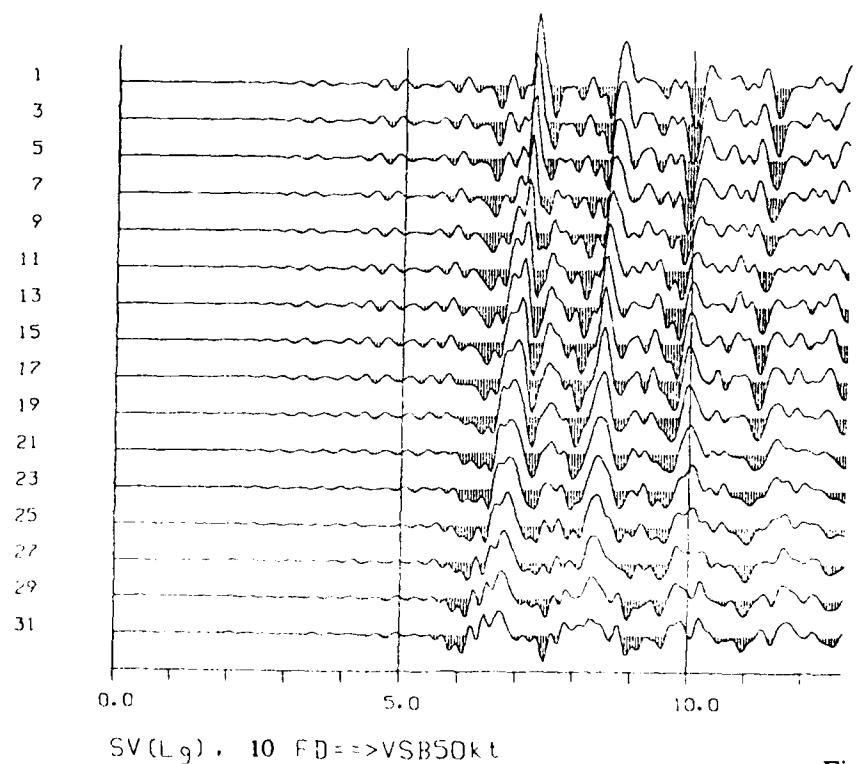
1
3
5
7
9
11
13
15
17
19
21
23
25
27
29
31
0.0
5.0
10.0
SV(Lg), 10 FD= =>VSB50kt

Fig. 20

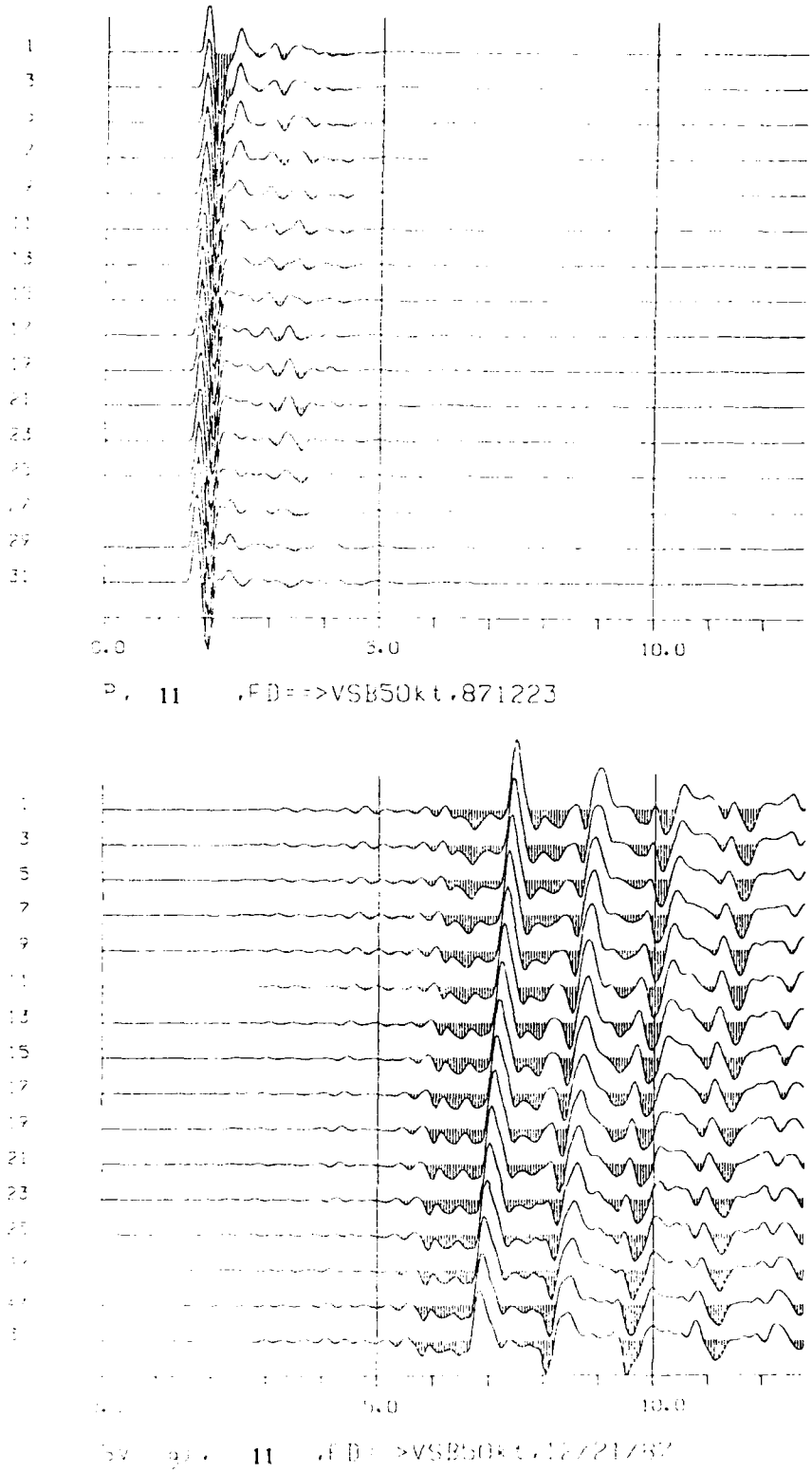
1
3
5
7
9
11
13
15
17
19
21
23
25
27
29
31
0.0
5.0
10.0
P, 11 ,FD=>VSB50kt,871223

Fig. 21

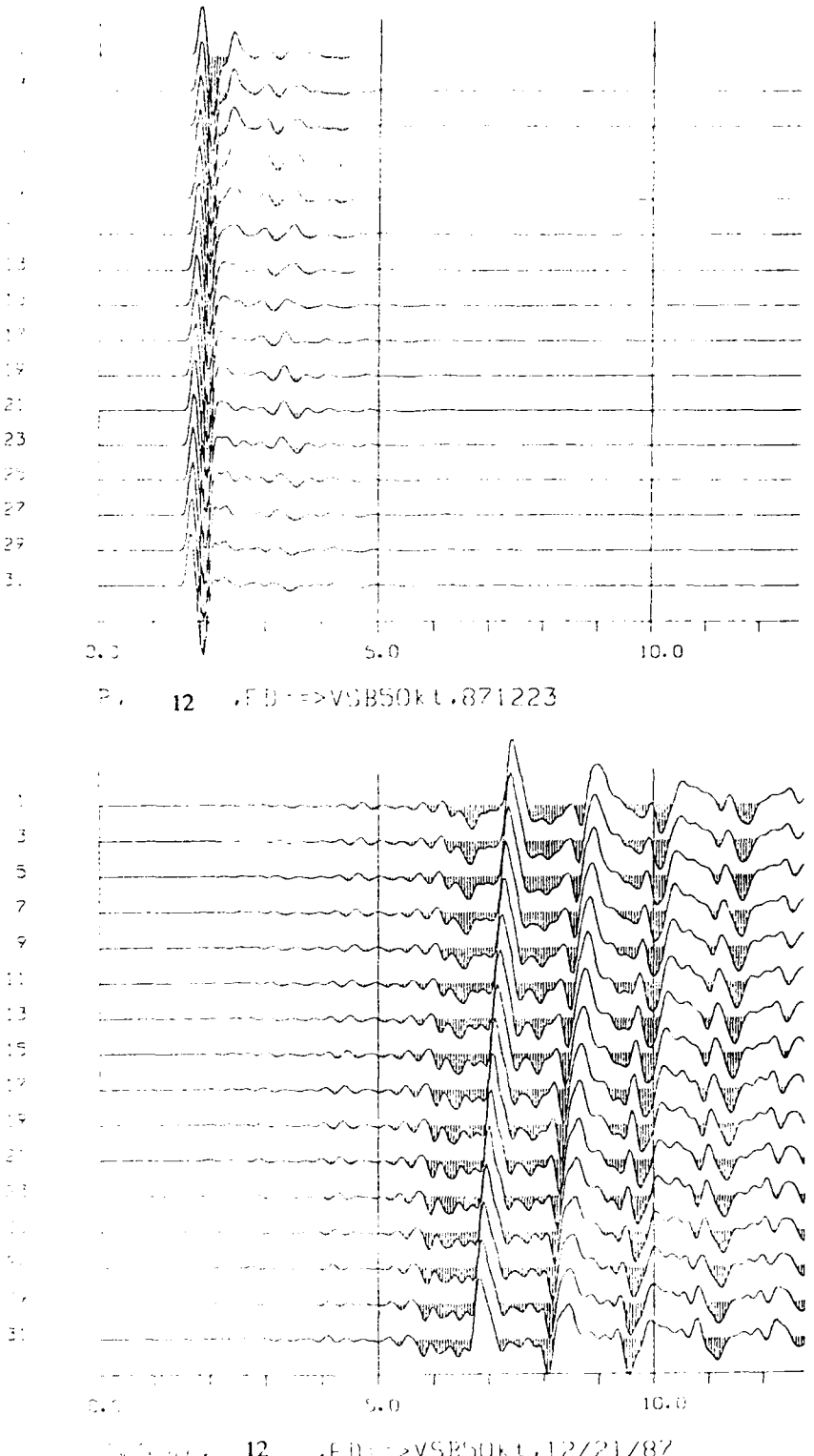

Fig. 22

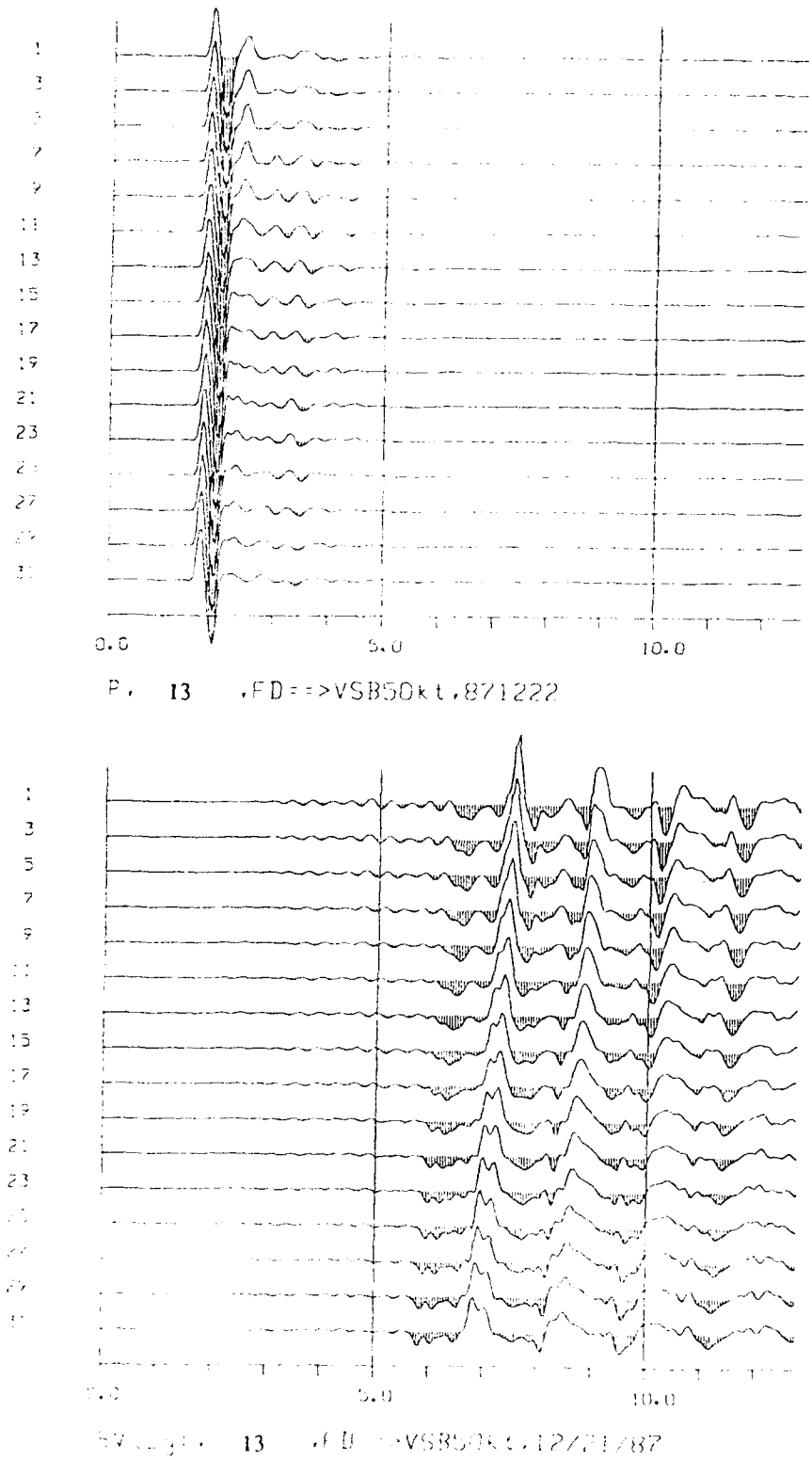
1
3
5
7
9
11
13
15
17
19
21
23
25
27
29
31
0.0
5.0
10.0
P, 13 ,FD==>VSB50kt,871222
1
3
5
7
9
11
13
15
17
19
21
23
25
27
29
31
0.0
5.0
10.0
SV_Lg, 13 ,FD==>VSB50kt,871222

Fig. 23

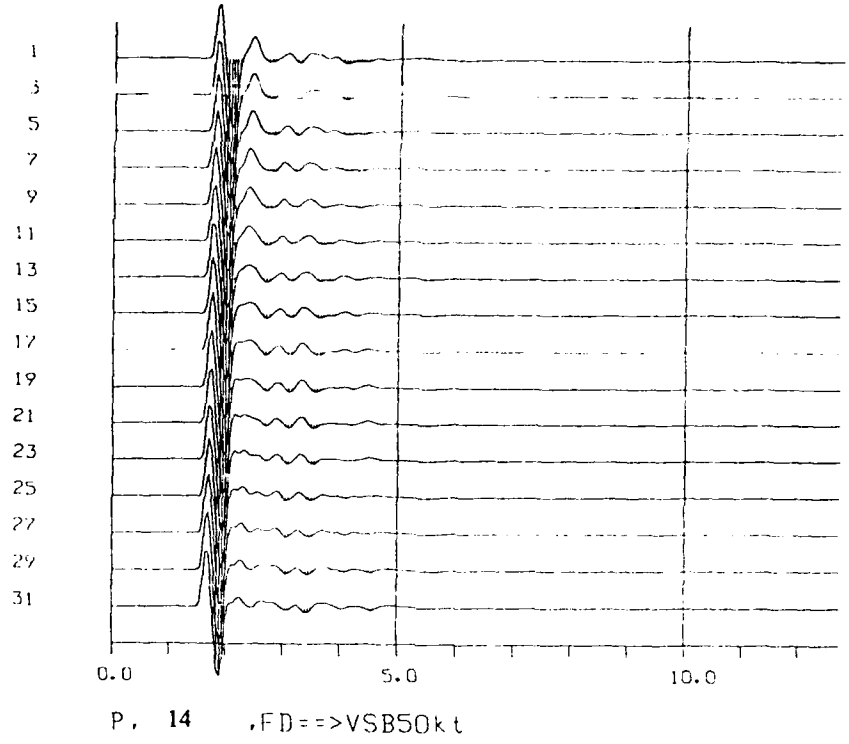
1
3
5
7
9
11
13
15
17
19
21
23
25
27
29
31
0.0
5.0
10.0
P, 14 ,FD==>VSB50kt

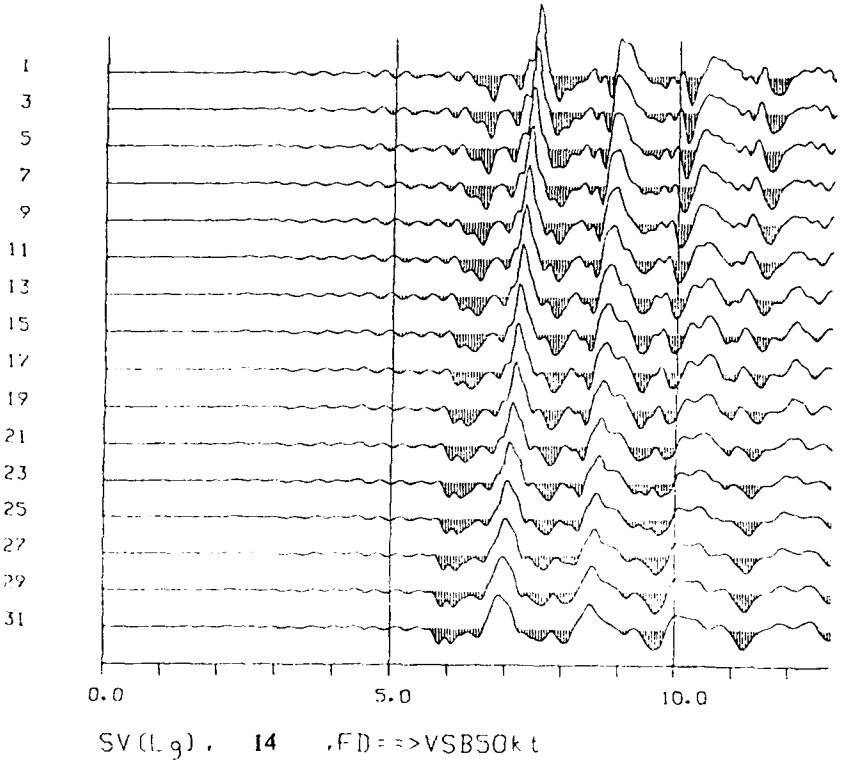
1
3
5
7
9
11
13
15
17
19
21
23
25
27
29
31
0.0
5.0
10.0
SV(Lg), 14 ,FD==>VSB50kt

Fig. 24

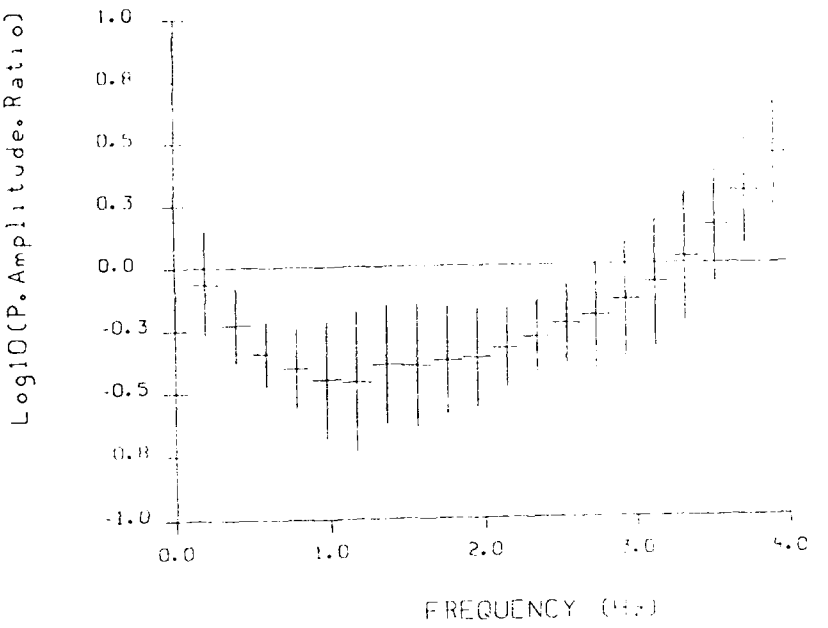
Log10(P.Amplitude.Ratio)
1.0
0.8
0.5
0.3
0.0
-0.3
-0.5
-0.8
-1.0
0.0
1.0
2.0
3.0
4.0
FREQUENCY (Hz)
P(I)/P(5+0%,2km,flat)

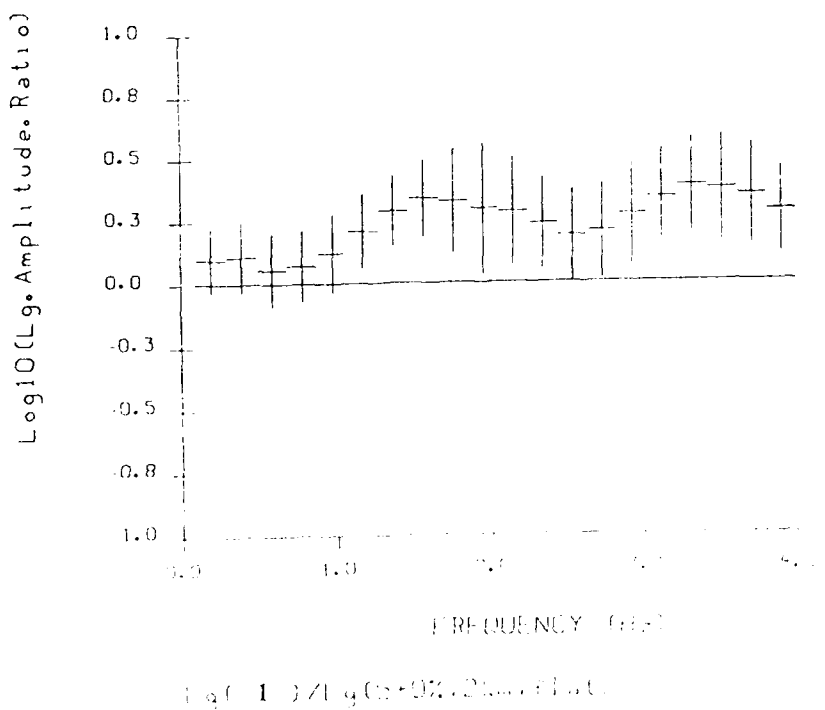
Log10(Lg.Amplitude.Ratio)
1.0
0.8
0.5
0.3
0.0
-0.3
-0.5
-0.8
1.0
FREQUENCY (Hz)

Fig. 25

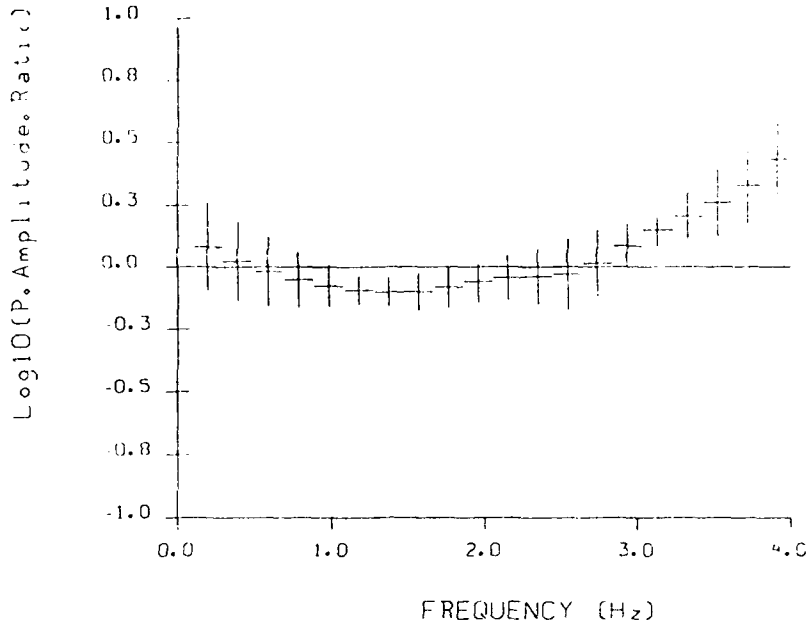
Log10(P.Amplitude.Ratio)
1.0
0.8
0.5
0.3
0.0
-0.3
-0.5
-0.8
-1.0
0.0
1.0
2.0
3.0
4.0
FREQUENCY (Hz)
P 2 /P(5+0%,2km,flat)

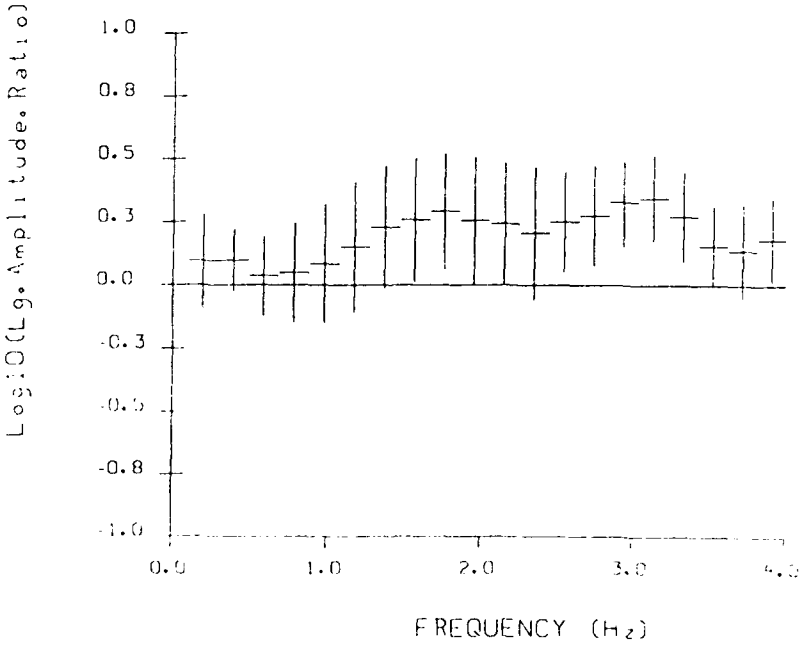
Log10(Lg.Amplitude.Ratio)
1.0
0.8
0.5
0.3
0.0
-0.3
-0.5
-0.8
-1.0
0.0
1.0
2.0
3.0
4.0
FREQUENCY (Hz)
Lg 2 /Lg(5+0%,2km,flat)

Fig. 26

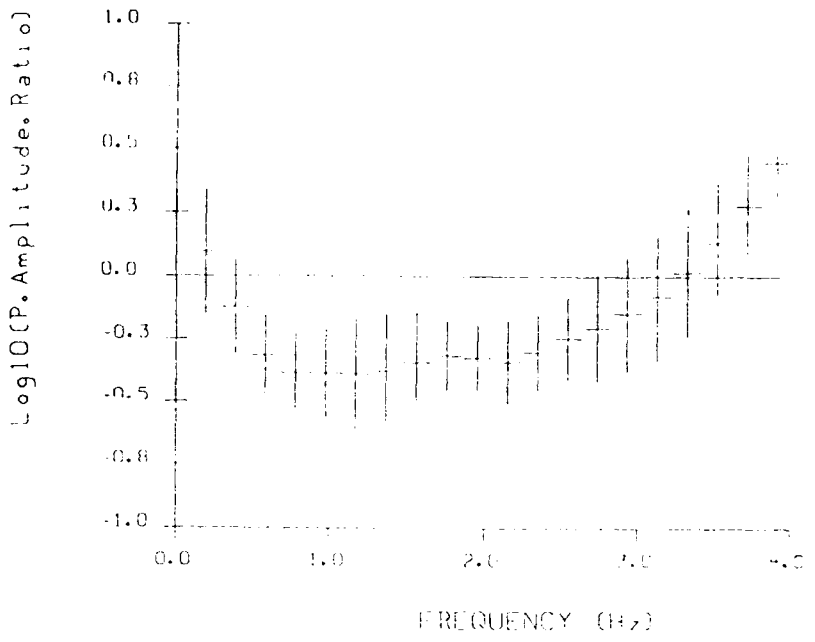
Log10(P.Amplitude.Ratio)
1.0
0.8
0.5
0.3
0.0
-0.3
-0.5
-0.8
-1.0
0.0
1.0
2.0
FREQUENCY (Hz)
P 3 /P(5.0%,2Km,flat)

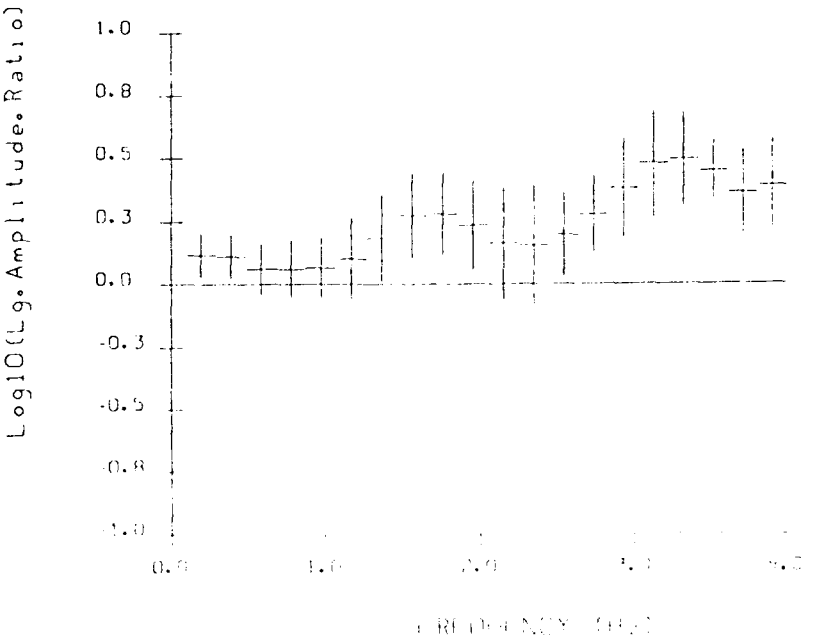
Log10(Lg.Amplitude.Ratio)
1.0
0.8
0.5
0.3
0.0
-0.3
-0.5
-0.8
0.0
1.0
2.0

Fig. 27

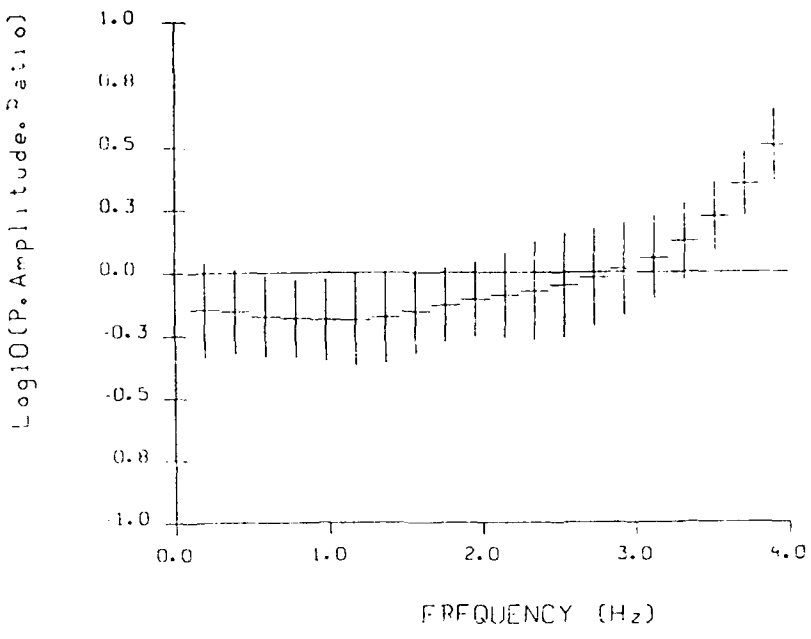

P(4)/P(5+0%,2km,flat)

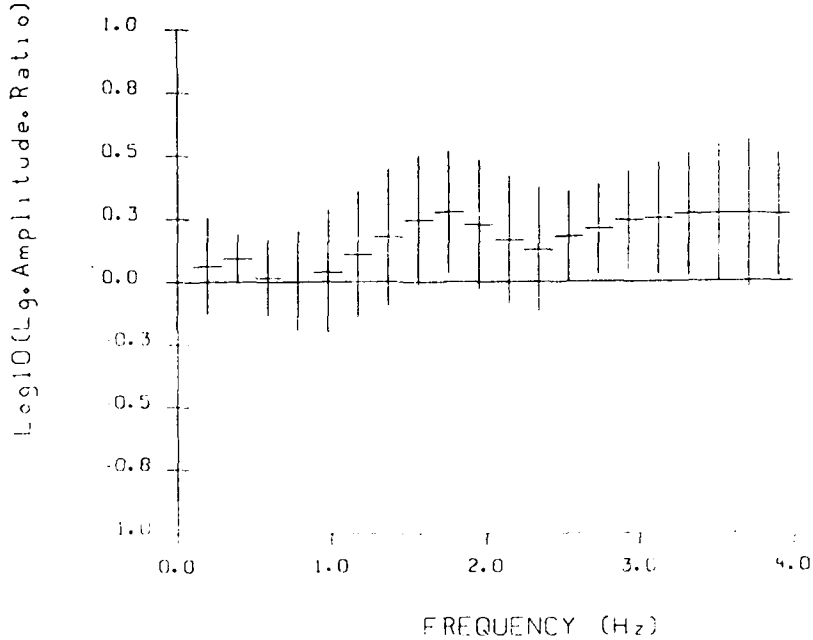

Lg 4 /Lg(5+0%,2km,flat)

Fig. 28

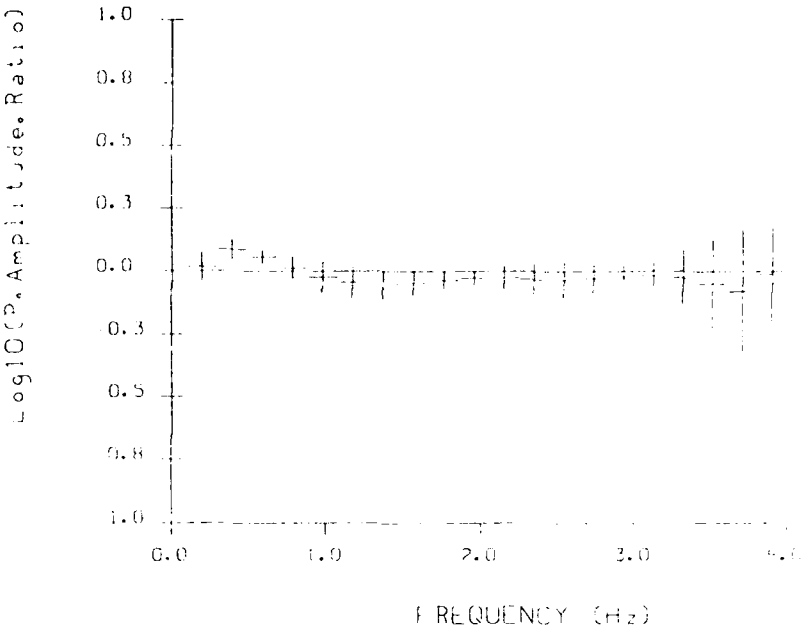
Log10(P.Amplitude.Ratio)
1.0
0.8
0.5
0.3
0.0
0.3
0.5
0.8
1.0
0.0
1.0
2.0
3.0
FREQUENCY (Hz)
P(S)/P(S+0%.2km.flat)

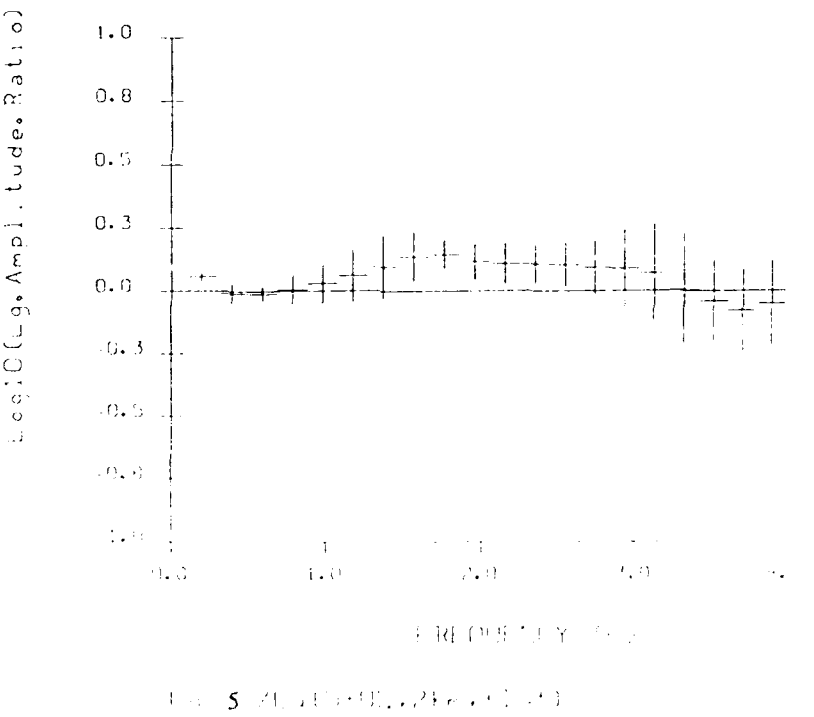
Log10(Lg.Ampl.tude.Ratio)
1.0
0.8
0.5
0.3
0.0
0.3
0.5
1.0
0.0
1.0
2.0
3.0

Fig. 29

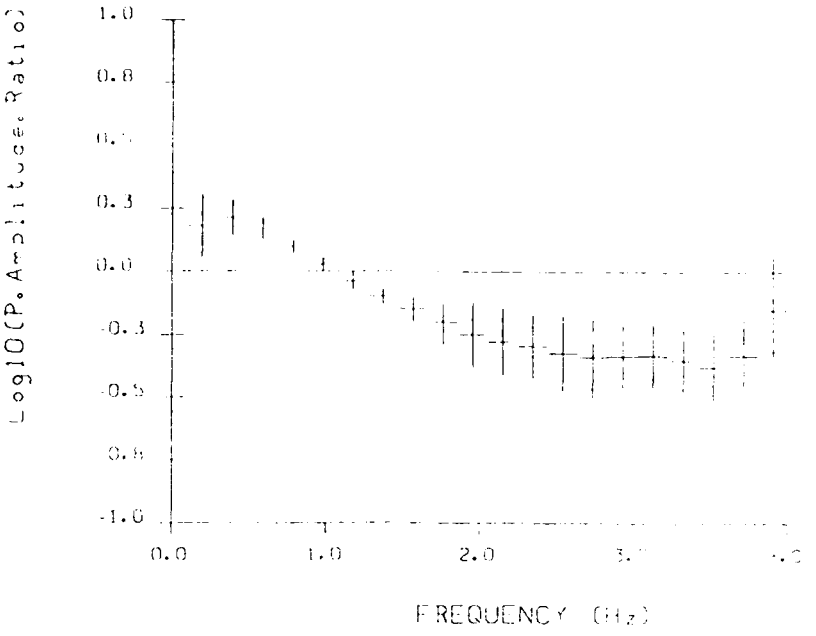

P(6)/P(5+0%,2km,flat)

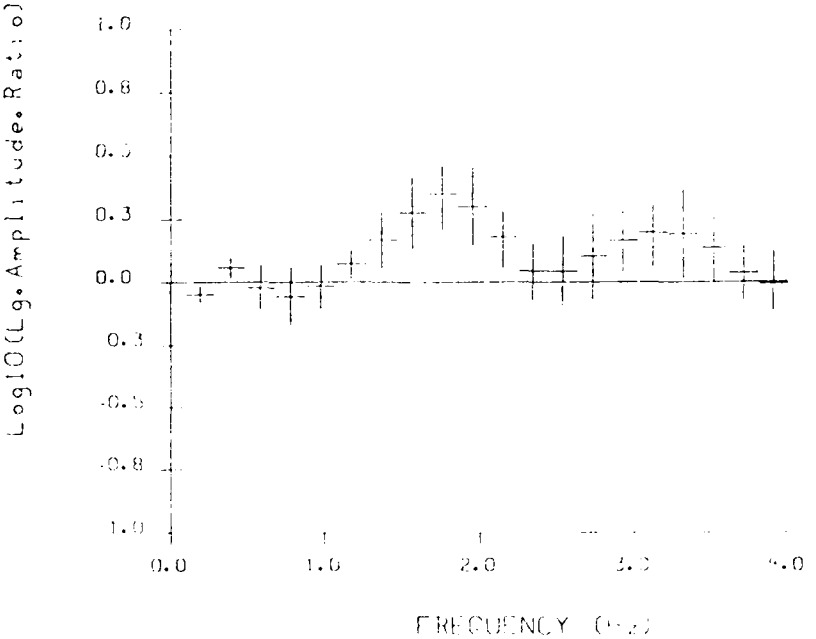

Lg(6)/Lg(5+0%,2km,flat)

Fig. 30

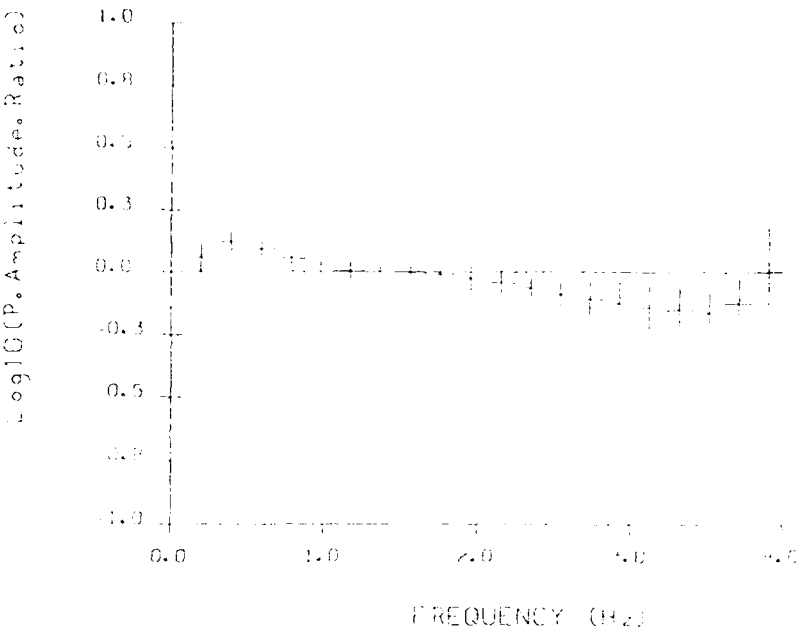

P(7)/P(5+0%,2km,flat)

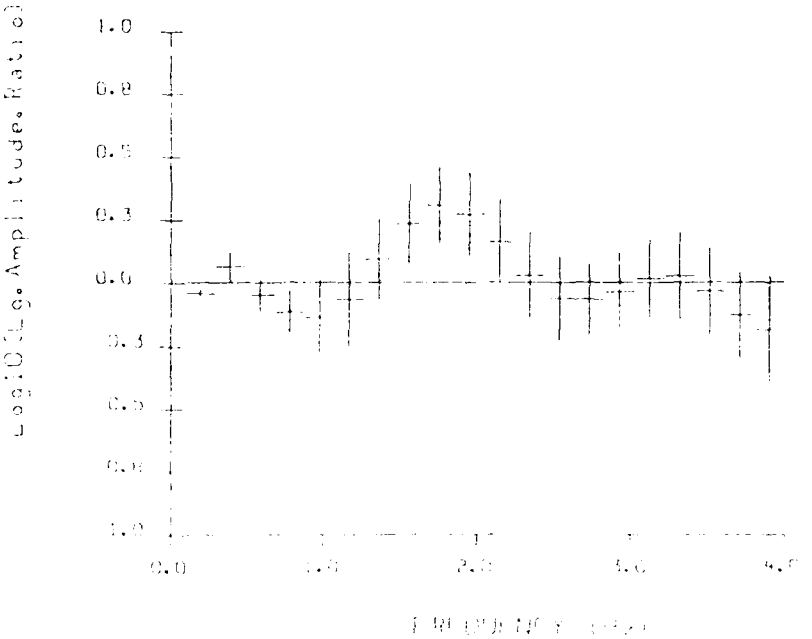

Fig. 31

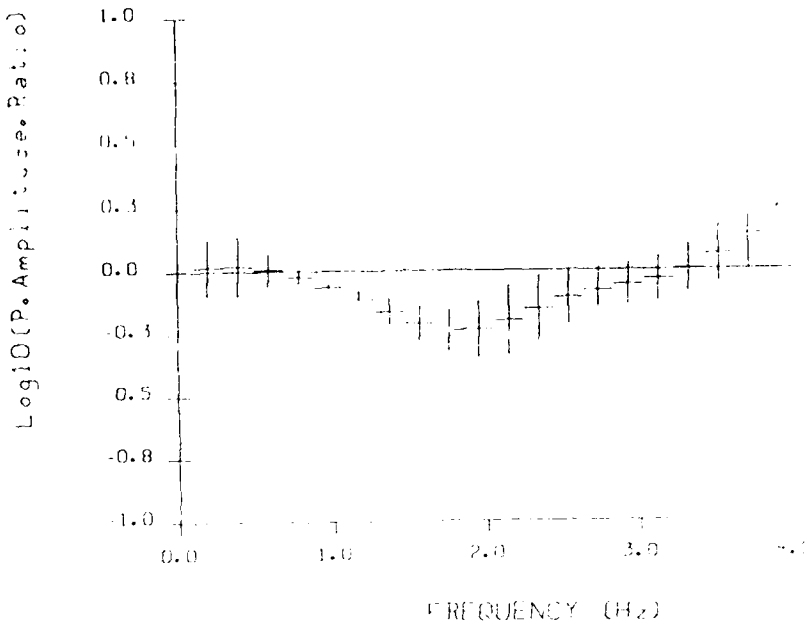

P-8 /PCS+0%.2km.flat)

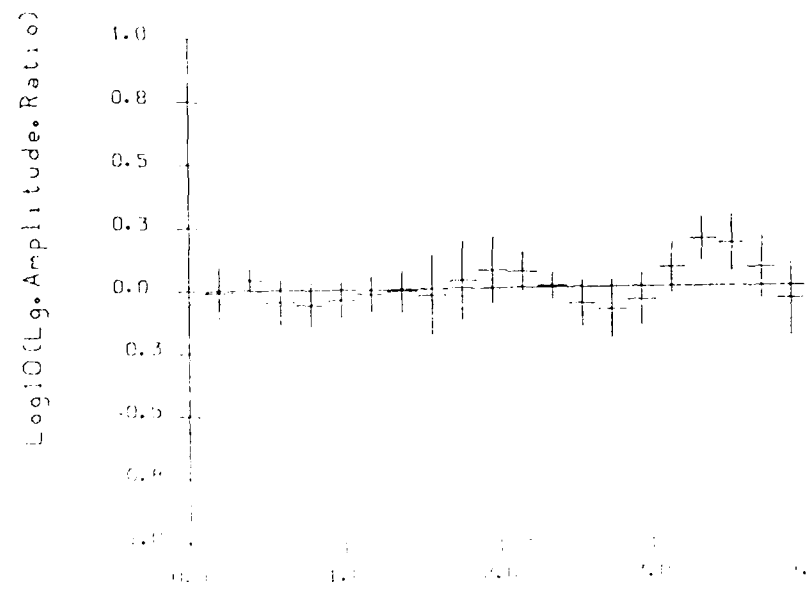

Fig. 32

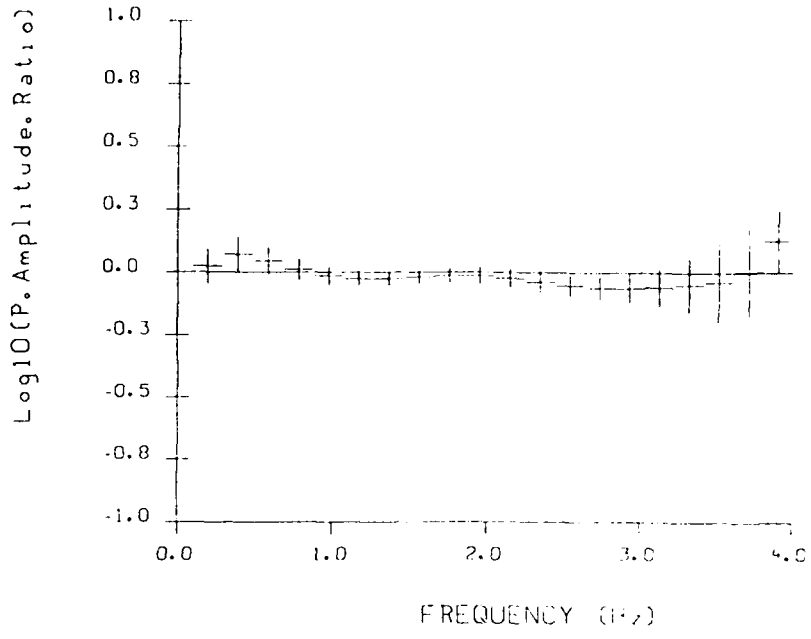

P(9)/P(5+0%,2km,flat)

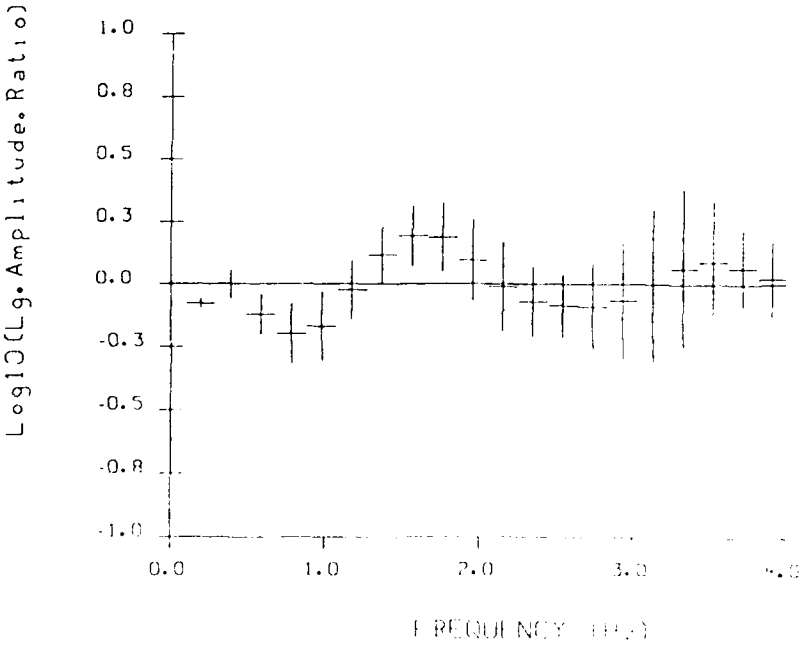

Lg(9)/Lg(5+0%,2km,flat)

Fig. 33

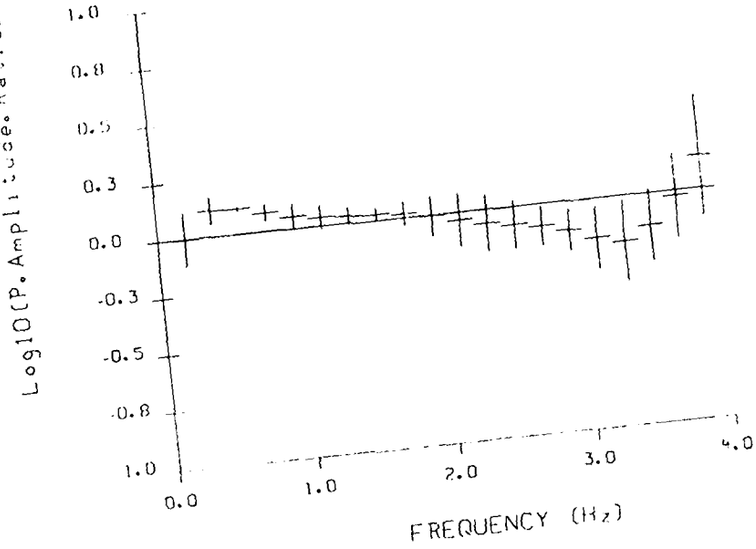

P 10 /P(5+0%.2km,flat)

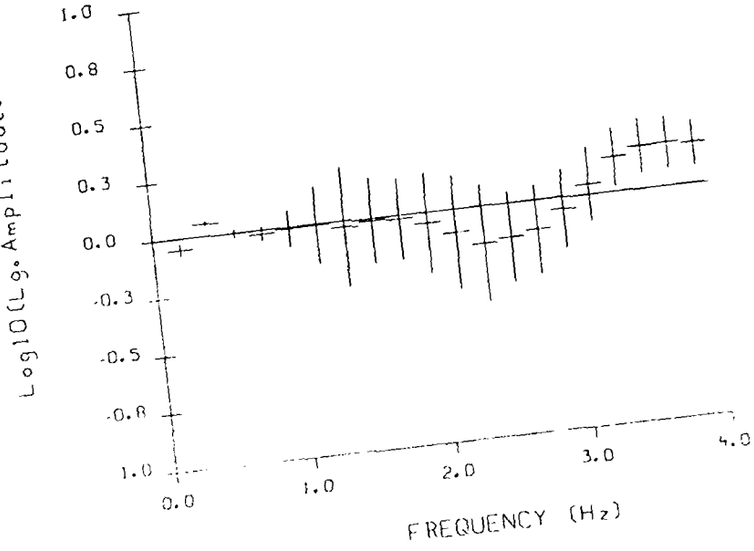

Lg 10 /Lg(5+0%.2km,flat)

Fig. 34

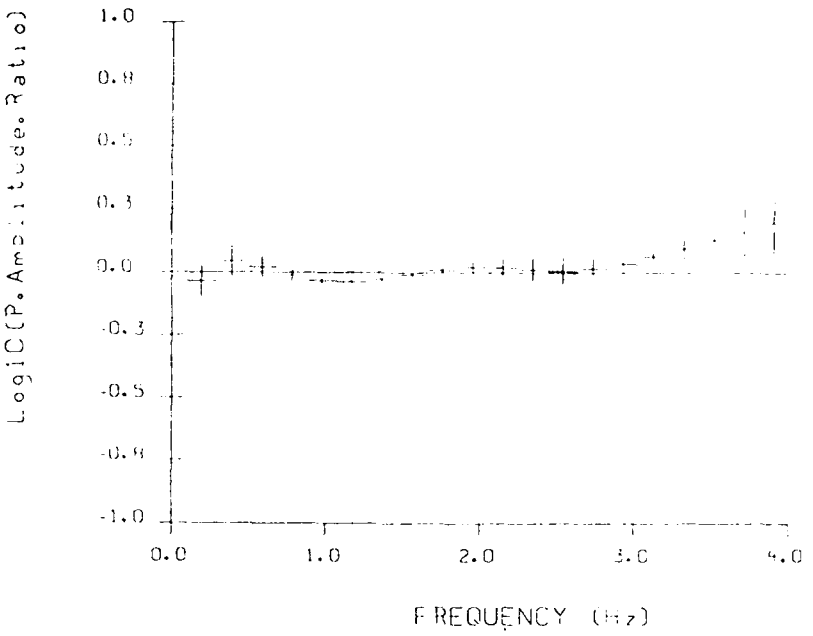

P(11)/P(5+0%.2km,flat)

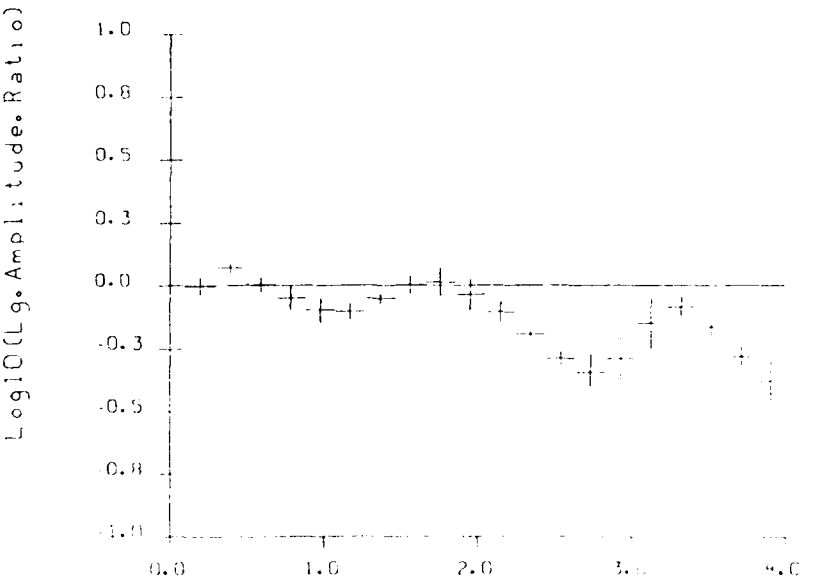

Fig. 35

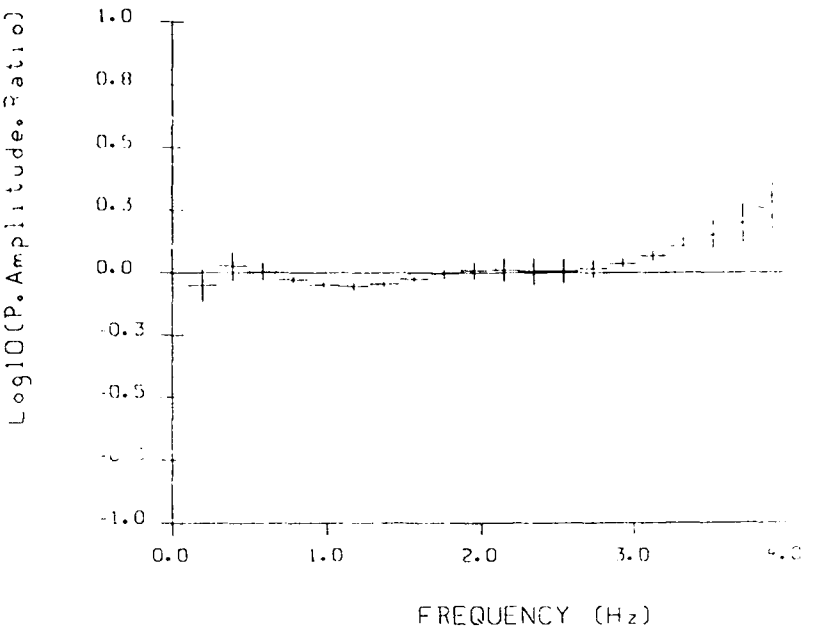

P(12)/P(5+0%,2km,flat)

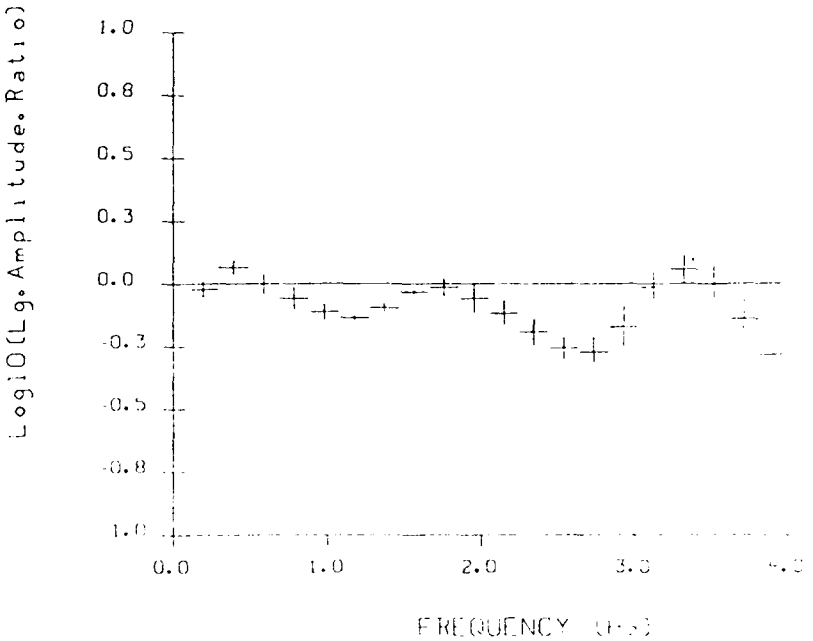

Lg(12)/Lg(5+0%,2km,flat)

Fig. 36

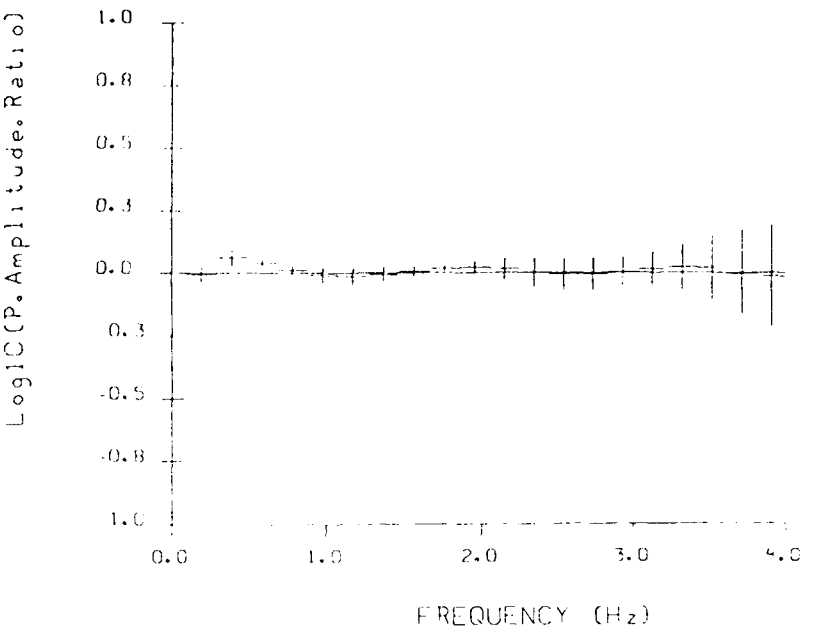

P(13)/P(5+0%,2km,flat)

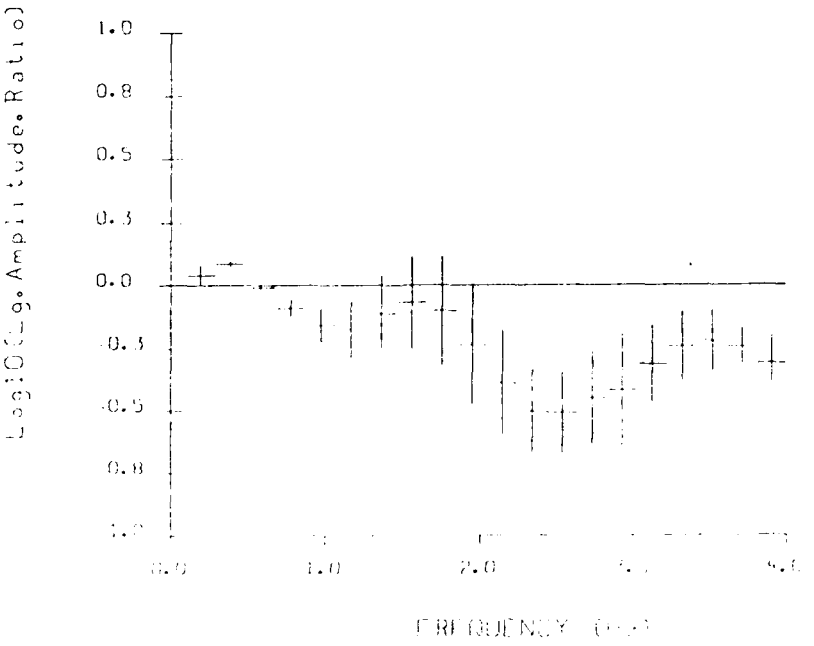

Lg(13)/Lg(5+0%,2km,flat)

Fig. 37

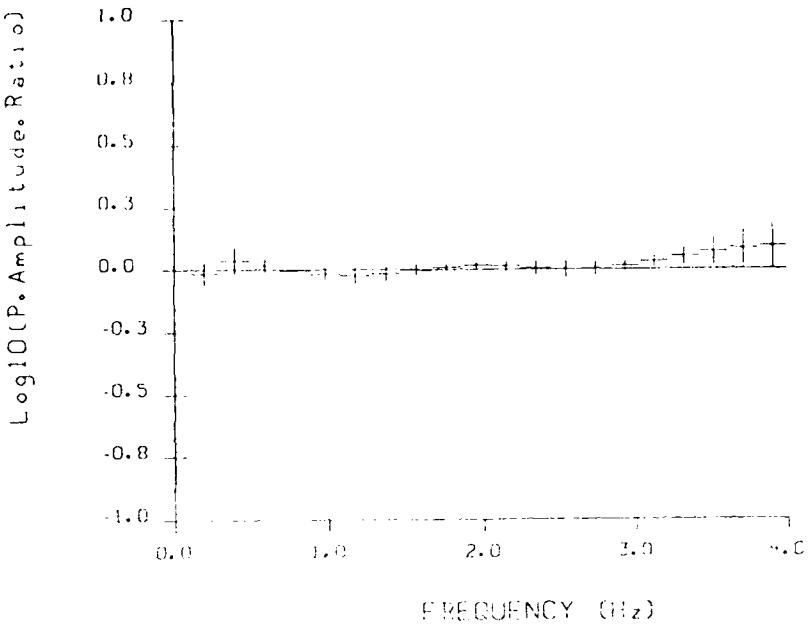

P(14)/P(5+0%,2km,flat)

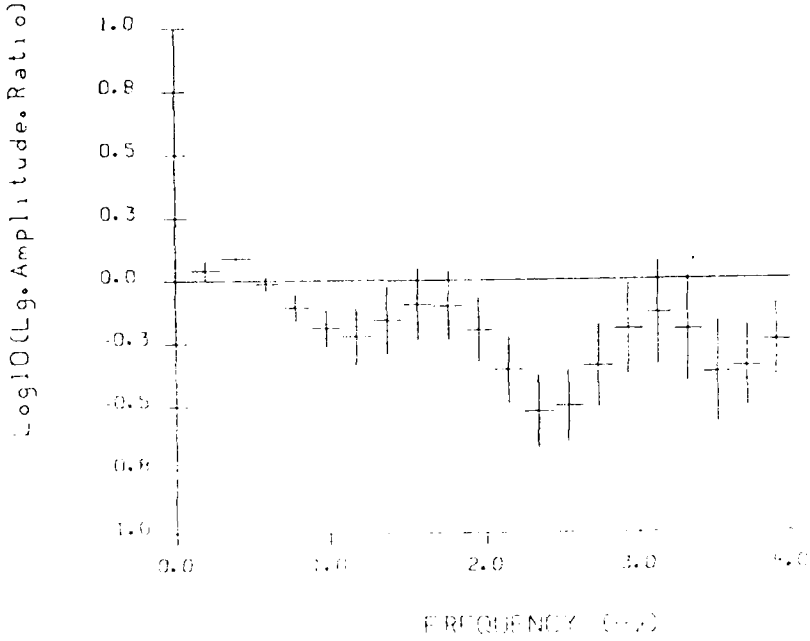

Lg 14)/Lg(5+0%,2km,flat)

Fig. 38

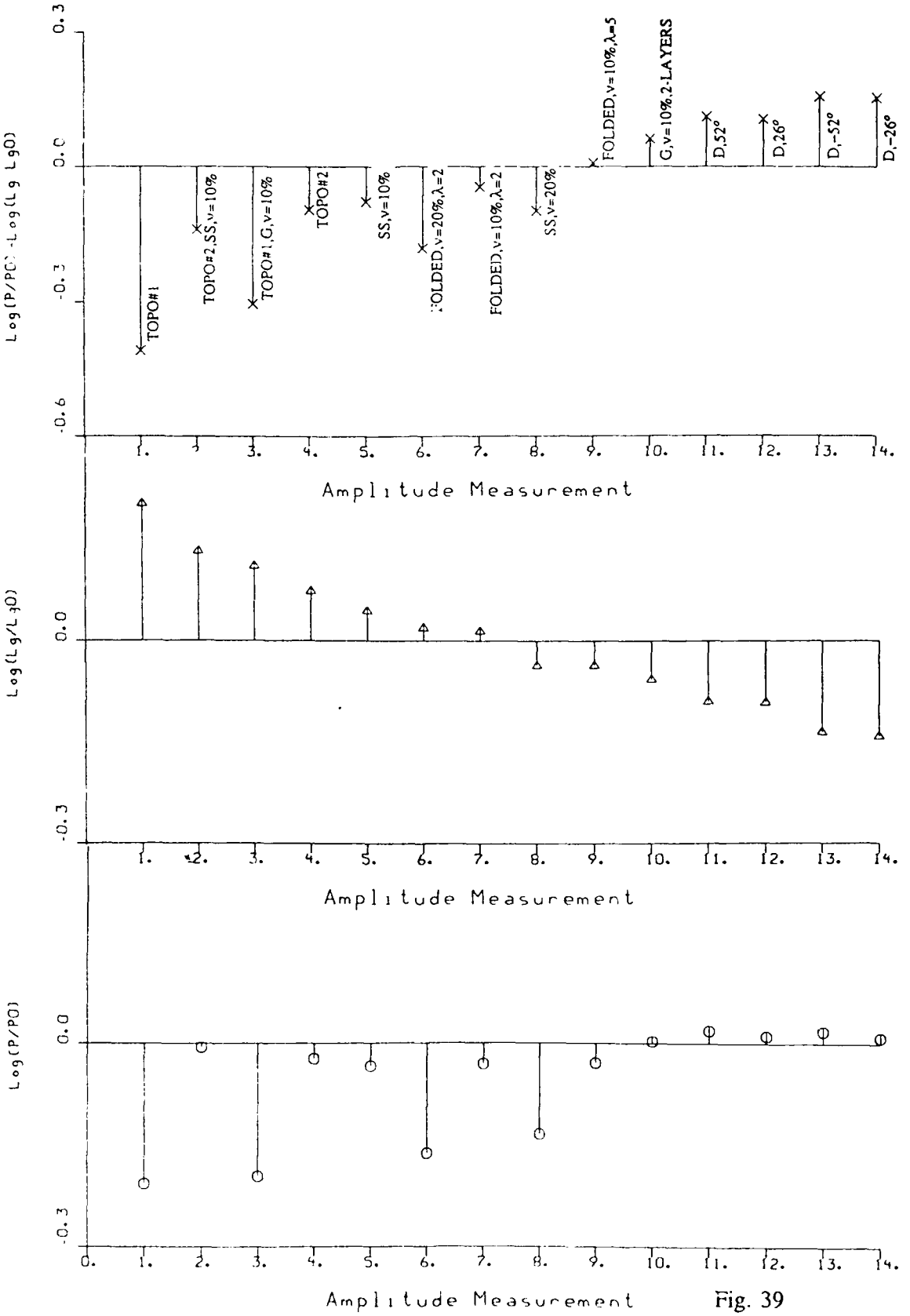
Log(P/PO)-Log(Lg Lg0)
0.3
0.0
-0.3
-0.6
TOPO#1
TOPO#2,SS,v=10%
TOPO#1,G,v=10%
TOPO#2
SS,v=10%
FOLDED,v=20%,λ=2
FOLDED,v=10%,λ=2
SS,v=20%
FOLDED,v=10%,λ=5
G,v=10%,2-LAYERS
D,52°
D,26°
D,-52°
D,-26°
1. 2. 3. 4. 5. 6. 7. 8. 9. 10. 11. 12. 13. 14.
Amplitude Measurement
Log(Lg/Lg0)
0.0
-0.3
1. 2. 3. 4. 5. 6. 7. 8. 9. 10. 11. 12. 13. 14.
Amplitude Measurement
Log(P/P0)
0.0
-0.3
0. 1. 2. 3. 4. 5. 6. 7. 8. 9. 10. 11. 12. 13. 14.
Amplitude Measurement

Fig. 39

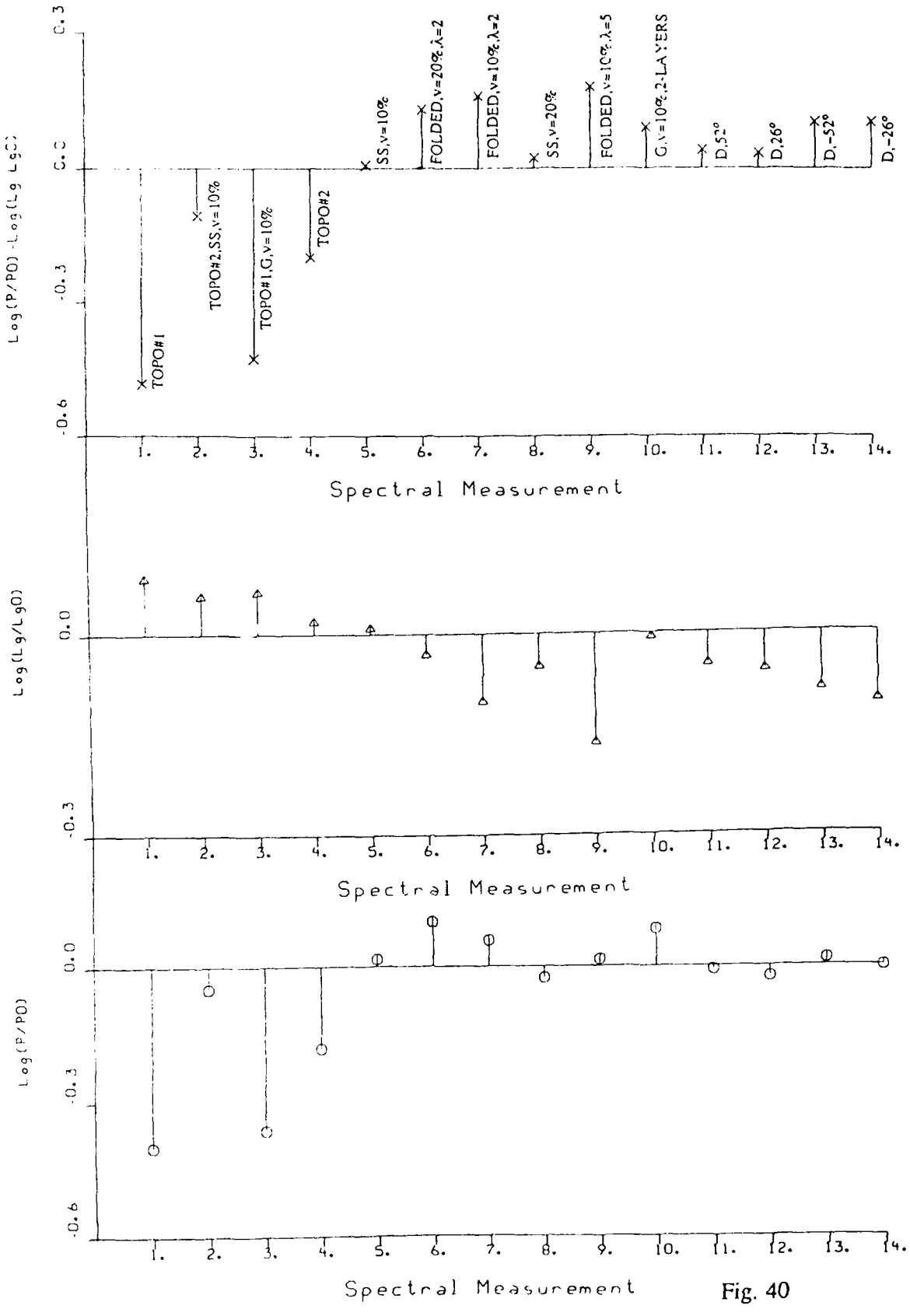
Log(P/PO)-Log(Lg Lg0)
0.3
0.0
-0.3
-0.6
TOPO#1
TOPO#2,SS,v=10%
TOPO#1,G,v=10%
TOPO#2
SS,v=10%
FOLDED,v=20%,λ=2
FOLDED,v=10%,λ=2
SS,v=20%
FOLDED,v=10%,λ=5
G,v=10%,2-LAYERS
D,52°
D,26°
D,-52°
D,-26°
1. 2. 3. 4. 5. 6. 7. 8. 9. 10. 11. 12. 13. 14.
Spectral Measurement
Log(Lg/Lg0)
0.0
-0.3
1. 2. 3. 4. 5. 6. 7. 8. 9. 10. 11. 12. 13. 14.
Spectral Measurement
Log(P/P0)
0.0
-0.3
-0.6
1. 2. 3. 4. 5. 6. 7. 8. 9. 10. 11. 12. 13. 14.
Spectral Measurement

Fig. 40

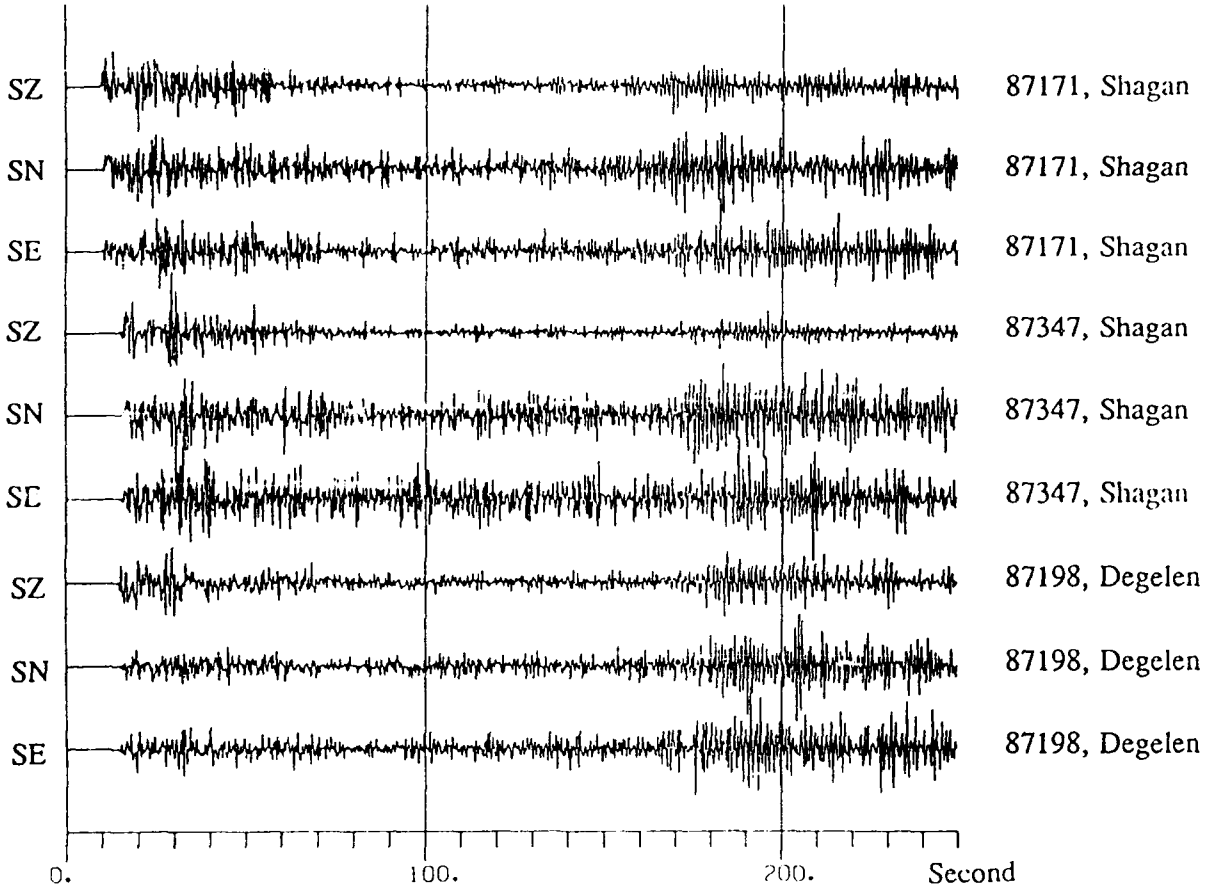

E. Kazakh Events, CDSN-WMQ

Fig. 41

Professor Keiiti Aki
Center for Earth Sciences
University of Southern California
University Park
Los Angeles, CA 90089-0741

Professor Charles B. Archambeau
Cooperative Institute for Resch
in Environmental Sciences
University of Colorado
Boulder, CO 80309

Dr. Thomas C. Bache Jr.
Science Applications Int'l Corp.
10210 Campus Point Drive
San Diego, CA 92121 (2 copies)

Dr. Douglas R. Baumgardt
Signal Analysis & Systems Div.
ENSCO, Inc.
5400 Port Royal Road
Springfield, VA 22151-2388

Dr. S. Bratt
Science Applications Int'l Corp.
10210 Campus Point Drive
San Diego, CA 92121

Dr. Lawrence J. Burdick
Woodward-Clyde Consultants
P.O. Box 93245
Pasadena, CA 91109-3245 (2 copies)

Professor Robert W. Clayton
Seismological Laboratory/Div. of
Geological & Planetary Sciences
California Institute of Technology
Pasadena, CA 91125

Dr. Vernon F. Cormier
Department of Geology & Geophysics
U-45, Room 207
The University of Connecticut
Storrs, Connecticut 06268

Dr. Zoltan A. Der
ENSCO, Inc.
5400 Port Royal Road
Springfield, VA 22151-2388

Professor John Ferguson
Center for Lithospheric Studies
The University of Texas at Dallas
P.O. Box 830688
Richardson, TX 75083-0688

Professor Stanley Flatte'
Applied Sciences Building
University of California, Santa Cruz
Santa Cruz, CA 95064

Professor Steven Grand
Department of Geology
245 Natural History Building
1301 West Green Street
Urbana, IL 61801

Professor Roy Greenfield
Geosciences Department
403 Deike Building
The Pennsylvania State University
University Park, PA 16802

Professor David G. Harkrider
Seismological Laboratory
Div of Geological & Planetary Sciences
California Institute of Technology
Pasadena, CA 91125

Professor Donald V. Helmberger
Seismological Laboratory
Div of Geological & Planetary Sciences
California Institute of Technology
Pasadena, CA 91125

Professor Eugene Herrin
Institute for the Study of Earth
& Man/Geophysical Laboratory
Southern Methodist University
Dallas, TX 75275

Professor Robert B. Herrmann
Department of Earth & Atmospheric
Sciences
Saint Louis University
Saint Louis, MO 63156

Professor Lane R. Johnson
Seismographic Station
University of California
Berkeley, CA 94720

Professor Thomas H. Jordan
Department of Earth, Atmospheric
and Planetary Sciences
Mass Institute of Technology
Cambridge, MA 02139

Dr. Alan Kafka
Department of Geology &
Geophysics
Boston College
Chestnut Hill, MA 02167

Professor Leon Knopoff
University of California
Institute of Geophysics
& Planetary Physics
Los Angeles, CA 90024

Professor Charles A. Langston
Geosciences Department
403 Deike Building
The Pennsylvania State University
University Park, PA 16802

Professor Thorne Lay
Department of Geological Sciences
1006 C.C. Little Building
University of Michigan
Ann Harbor, MI 48109-1063

Dr. Randolph Martin III
New England Research, Inc.
P.O. Box 857
Norwich, VT 05055

Dr. Gary McCartor
Mission Research Corp.
735 State Street
P.O. Drawer 719
Santa Barbara, CA 93102 (2 copies)

Professor Thomas V. McEvilly
Seismographic Station
University of California
Berkeley, CA 94720

Dr. Keith L. McLaughlin
Teledyne Geotech
314 Montgomery Street
Alexandria, VA 22314

Professor William Menke
Lamont-Doherty Geological Observatory
of Columbia University
Palisades, NY 10964

Professor Brian J. Mitchell
Department of Earth & Atmospheric
Sciences
Saint Louis University
Saint Louis, MO 63156

Mr. Jack Murphy
S-CUBED
A Division of Maxwell Laboratory
11800 Sunrise Valley Drive
Suite 1212
Reston, VA 22091 (2 copies)

Professor Otto W. Nuttli
Department of Earth &
Atmospheric Sciences
Saint Louis University
Saint Louis, MO 63156

Professor J. A. Orcutt
Institute of Geophysics and Planetary
Physics, A-205
Scripps Institute of Oceanography
Univ. of California, San Diego
La Jolla, CA 92093

Professor Keith Priestley
University of Nevada
Mackay School of Mines
Reno, Nevada 89557

Professor Charles G. Sammis
Center for Earth Sciences
University of Southern California
University Park
Los Angeles, CA 90089-0741

Dr. Jeffrey L. Stevens
S-CUBED,
A Division of Maxwell Laboratory
P.O. Box 1620
La Jolla, CA 92038-1620

Professor Brian Stump
Institute for the Study of Earth & Man
Geophysical Laboratory
Southern Methodist University
Dallas, TX 75275

Professor Ta-liang Teng
Center for Earth Sciences
University of Southern California
University Park
Los Angeles, CA 90089-0741

Professor M. Nafi Toksoz
Earth Resources Lab
Dept of Earth, Atmospheric and
Planetary Sciences
Massachusetts Institute of Technology
42 Carleton Street
Cambridge, MA 02142

Professor Terry C. Wallace
Department of Geosciences
Building #11
University of Arizona
Tucson, AZ 8[illegible]21

Professor Francis T. Wu
Department of Geological Sciences
State University of new York
At Binghamton
Vestal, NY 13901

OCT87

OTHERS (United States)

Dr. Monem Abdel-Gawad
Rockwell Internat'l Science Center
1049 Camino Dos Rios
Thousand Oaks, CA 91360

Professor Shelton S. Alexander
Geosciences Department
403 Deike Building
The Pennsylvania State University
University Park, PA 16802

Dr. Muawia Barazangi
Geological Sciences
Cornell University
Ithaca, NY 14853

Mr. William J. Best
907 Westwood Drive
Vienna, VA 22180

Dr. N. Biswas
Geophysical Institute
University of Alaska
Fairbanks, AK 99701

Dr. G. A. Bollinger
Department of Geological Sciences
Virginia Polytechnical Institute
21044 Derring Hall
Blacksburg, VA 24061

Dr. James Bulau
Rockwell Int'l Science Center
1049 Camino Dos Rios
P.O. Box 1085
Thousand Oaks, CA 91360

Mr. Roy Burger
1221 Serry Rd.
Schenectady, NY 12309

Dr. Robert Burridge
Schlumberger-Doll Resch Ctr.
Old Quarry Road
Ridgefield, CT 06877

Science Horizons, Inc.
ATTN: Dr. Theodore Cherry
710 Encinitas Blvd., Suite 101
Encinitas, CA 92024 (2 copies)

Professor Jon F. Claerbout

Professor Amos Nur
Dept. of Geophysics
Stanford University
Stanford, CA 94305 (2 copies)

Dr. Anton W. Dainty
AFGL/LWH
Hanscom AFB, MA 01731

Professor Adam Dziewonski
Hoffman Laboratory
Harvard University
20 Oxford St.
Cambridge, MA 02138

Professor John Ebel
Dept of Geology & Geophysics
Boston College
Chestnut Hill, MA 02167

Dr. Alexander Florence
SRI International
333 Ravenwood Avenue
Menlo Park, CA 94025-3493

Dr. Donald Forsyth
Dept. of Geological Sciences
Brown University
Providence, RI 02912

Dr. Anthony Gangi
Texas A&M University
Department of Geophysics
College Station, TX 77843

Dr. Freeman Gilbert
Institute of Geophysics &
Planetary Physics
Univ. of California, San Diego
P.O. Box 109
La Jolla, CA 92037

Mr. Edward Giller
Pacific Seirra Research Corp.
1401 Wilson Boulevard
Arlington, VA 22209

Dr. Jeffrey W. Given
Sierra Geophysics
11255 Kirkland Way
Kirkland, WA 98033

Dr. Arthur Lerner-Lam
Lamont-Doherty Geological Observatory
of Columbia University
Palisades, NY 10964

Dr. L. Timothy Long
School of Geophysical Sciences
Georgia Institute of Technology
Atlanta, GA 30332

Dr. George R. Mellman
Sierra Geophysics
11255 Kirkland Way
Kirkland, WA 98033

Dr. Bernard Minster
Institute of Geophysics and Planetary
Physics, A-205
Scripps Institute of Oceanography
Univ. of California, San Diego
La Jolla, CA 92093

Dr. Geza Nagy
SRI International
333 Ravenswood Avenue
Menlo Park, CA 94025-3493

Dr. Jack Oliver
Department of Geology
Cornell University
Ithaca, NY 14850

Dr. Robert Phinney/Dr. F.A. Dahlen
Dept of Geological
Geophysical Sci. University
Princeton University
Princeton, NJ 08540 (2 copies)

Professor Paul G. Richards
Lamont-Doherty Geological
Observatory of Columbia Univ.
Palisades, NY 10964

Dr. Norton Rimer
S-CUBED
A Division of Maxwell Laboratory
P.O. 1620
La Jolla, CA 92038-1620

Professor Larry J. Ruff
Department of Geological Sciences
1006 C.C. Little Building
University of Michigan
Ann Arbor, MI 48109-1063

Dr. Alan S. Ryall, Jr.
Center of Seismic Studies
1300 North 17th Street
Suite 1450
Arlington, VA 22209-2308 (4 copies)

Dr. David G. Simpson
Lamont-Doherty Geological Observ.
of Columbia University
Palisades, NY 10964

Dr. Bob Smith
Department of Geophysics
University of Utah
1400 East 2nd South
Salt Lake City, UT 84112

Dr. S. W. Smith
Geophysics Program
University of Washington
Seattle, WA 98195

Rondout Associates
ATTN: Dr. George Sutton,
Dr. Jerry Carter, Dr. Paul Pomeroy
P.O. Box 224
Stone Ridge, NY 12484 (4 copies)

Dr. L. Sykes
Lamont Doherty Geological Observ.
Columbia University
Palisades, NY 10964

Dr. Pradeep Talwani
Department of Geological Sciences
University of South Carolina
Columbia, SC 29208

Dr. R. B. Tittmann
Rockwell International Science Center
1049 Camino Dos Rios
P.O. Box 1085
Thousand Oaks, CA 91360

Weidlinger Associates
ATTN: Dr. Gregory Wojcik
620 Hansen Way, Suite 100
Palo Alto, CA 94304

Professor John H. Woodhouse
Hoffman Laboratory
Harvard University
20 Oxford St.
Cambridge, MA 02138

Dr. Gregory B. Young
ENSCO, Inc.
5400 Port Royal Road
Springfield, VA 22151-2388

Dr. Peter Basham
Earth Physics Branch
Geological Survey of Canada
1 Observatory Crescent
Ottawa, Ontario
CANADA K1A 0Y3

Dr. Eduard Berg
Institute of Geophysics
University of Hawaii
Honolulu, HI 96822

Dr. Michel Bouchon - Universite
Scientifique et Medicale de Grenob
Lab de Geophysique - Interne et
Tectonophysique - I.R.I.G.M-B.P.
38402 St. Martin D'Heres
Cedex FRANCE

Dr. Hilmar Bungum/NTNF/NORSAR
P.O. Box 51
Norwegian Council of Science,
Industry and Research, NORSAR
N-2007 Kjeller, NORWAY

Dr. Michel Campillo
I.R.I.G.M.-B.P. 68
38402 St. Martin D'Heres
Cedex, FRANCE

Dr. Kin-Yip Chun
Geophysics Division
Physics Department
University of Toronto
Ontario, CANADA M5S 1A7

Dr. Alan Douglas
Ministry of Defense
Blacknest, Brimpton,
Reading RG7-4RS
UNITED KINGDOM

Dr. Manfred Henger
Fed. Inst. For Geosciences & Nat'l Res.
Postfach 510153
D-3000 Hannover 51
FEDERAL REPUBLIC OF GERMANY

Dr. E. Husebye
NTNF/NORSAR
P.O. Box 51
N-2007 Kjeller, NORWAY

Tormod Kvaerna
NTNF/NORSAR
P.O. Box 51
N-2007 Kjeller, NORWAY

OCT87

Mr. Peter Marshall, Procurement
Executive, Ministry of Defense
Blacknest, Brimpton,
Reading FG7-4RS
UNITED KINGDOM (3 copies)

Dr. Ben Menaheim
Weizman Institute of Science
Rehovot, ISRAEL 951729

Dr. Svein Mykkeltveit
NTNF/NORSAR
P.O. Box 51
N-2007 Kjeller, NORWAY (3 copies)

Dr. Robert North
Geophysics Division
Geological Survey of Canada
1 Observatory crescent
Ottawa, Ontario
CANADA, K1A OY3

Dr. Frode Ringdal
NTNF/NORSAR
P.O. Box 51
N-2007 Kjeller, NORWAY

Dr. Jorg Schlittenhardt
Federal Inst. for Geosciences & Nat'l Res.
Postfach 510153
D-3000 Hannover 51
FEDERAL REPUBLIC OF GERMANY

University of Hawaii
Institute of Geophysics
ATTN: Dr. Daniel Walker
Honolulu, HI 96822

Dr. Ramon Cabre, S.J.
c/o Mr. Ralph Buck
Economic Consular
American Embassy
APO Miami, Florida 34032

Professor Peter Harjes
Institute for Geophysik
Rhur University/Bochum
P.O. Box 102148, 4630 Bochum 1
FEDERAL REPUBLIC OF GERMANY

Professor Brian L.N. Kennett
Research School of Earth Sciences
Institute of Advanced Studies
G.P.O. Box 4
Canberra 2601
AUSTRALIA

Dr. B. Massinon
Societe Radiomana
27, Rue Claude Bernard
7,005, Paris, FRANCE (2 copies)

Dr. Pierre Mechler
Societe Radiomana
27, Rue Claude Bernard
75005, Paris, FRANCE

Dr. Ralph Alewine III
DARPA/NMRO
1400 Wilson Boulevard
Arlington, VA 22209-2308

Dr. Peter Basham
Geological Survey of Canada
1 Observatory Creseut
Ottowa, Ontario
CANADA K1A OY3

Dr. Robert Blandford
DARPA/NMRO
1400 Wilson Boulevard
Arlington, VA 22209-2308

Sandia National Laboratory
ATTN: Dr. H. B. Durham
Albuquerque, NM 87185

Dr. Jack Evernden
USGS-Earthquake Studies
345 Middlefield Road
Menlo Park, CA 94025

U.S. Geological Survey
ATTN: Dr. T. Hanks
Nat'l Earthquake Resch Center
345 Middlefield Road
Menlo Park, CA 94025

Dr. James Hannon
Lawrence Livermore Nat'l Lab.
P.O. Box 808
Livermore, CA 94550

U.S. Arms Control & Disarm. Agency
ATTN: Mrs. M. Hoinkes
Div. of Multilateral Affairs
Room 5499
Washington, D.C. 20451

Paul Johnson
ESS-4, Mail Stop J979
Los Alamos National Laboratory
Los Alamos, NM 87545

Ms. Ann Kerr
DARPA/NMRO
1400 Wilson Boulevard
Arlington, VA 22209-2308

Dr. Max Koontz
US Dept of Energy/DP 331
Forrestal Building
1000 Independence Ave.
Washington, D.C. 20585

Dr. W. H. K. Lee
USGS
Office of Earthquakes, Volcanoes,
& Engineering
Branch of Seismology
345 Middlefield Rd
Menlo Park, CA 94025

Dr. William Leith
USGS
Mail Stop 928
Reston, VA 22092

Dr. Robert Masse'
Box 25046, Mail Stop 967
Denver Federal Center
Denver, Colorado 80225

Dr. Keith K. Nakanishi
Lawrence Livermore National Laboratory
P.O. Box 808, L-205
Livermore, CA 94550 (2 copies)

Dr. Carl Newton
Los Alamos National Lab.
P.O. Box 1663
Mail Stop C335, Group E553
Los Alamos, NM 87545

Dr. Kenneth H. Olsen
Los Alamos Scientific Lab.
Post Office Box 1663
Los Alamos, NM 87545

Howard J. Patton
Lawrence Livermore National Laboratory
P.O. Box 808, L-205
Livermore, CA 94550

HQ AFTAC/TT
Attn: Dr. Frank F. Pilotte
Patrick AFB, Florida 32925-6001

Mr. Jack Rachlin
USGS - Geology, Rm 3 C136
Mail Stop 928 National Center
Reston, VA 22092

Robert Reinke
AFWL/NTESG
Kirtland AFB, NM 87117-6008

HQ AFTAC/TGR
Attn: Dr. George H. Rothe
Patrick AFB, Florida 32925-6001

Donald L. Springer
Lawrence Livermore National Laboratory
P.O. Box 808, L-205
Livermore, CA 94550

Dr. Lawrence Turnbull
OSWR/NED
Central Intelligence Agency
CIA, Room 5G48
Washington, D.C. 20505

Dr. Thomas Weaver
Los Alamos Scientific Laboratory
Los Almos, NM 97544

AFGL/SULL
Research Library
Hanscom AFB, MA 01731-5000 (2 copies)

Secretary of the Air Force (SAFRD)
Washington, DC 20330
Office of the Secretary Defense
DDR & E
Washington, DC 20330

HQ DNA
ATTN: Technical Library
Washington, DC 20305

Director, Technical Information
DARPA
1400 Wilson Blvd.
Arlington, VA 22209

AFGL/XO
Hanscom AFB, MA 01731-5000

AFGL/LW
Hanscom AFB, MA 01731-5000

DARPA/PM
1400 Wilson Boulevard
Arlington, VA 22209

Defense Technical
Information Center
Cameron Station
Alexandria, VA 22314
(12 copies)

Defense Intelligence Agency
Directorate for Scientific &
Technical Intelligence
Washington, D.C. 20301

Defense Nuclear Agency/SPSS
ATTN: Dr. Michael Shore
6801 Telegraph Road
Alexandria, VA 22310

AFOSR/NPG
ATTN: Major John Prince
Bldg 410, Room C222
Bolling AFB, Wash D.C. 20332

AFTAC/CA (STINFO)
Patrick AFB, FL 32925-6001